Wave Propagation Approach for Elastic Transient Reponses of Transversely Isotropic Asphalt Pavement under an Impact Load: A Semi Analytical Solution

Zejiao Dong[1], Weiwen Quan[2], Xianyong Ma[3], Liping Cao[4], Hongliang Zhang[5], and Zhen Leng[6]

[1]Professor, School of Transportation Science and Engineering, Harbin Institute of Technology, Harbin 150090, China. Email: hitdzj@hit.edu.cn

[2]PhD, School of Transportation Science and Engineering, Harbin Institute of Technology, Harbin 150090, China. Email: qww32102@hit.edu.cn

[3]PhD, School of Transportation Science and Engineering, Harbin Institute of Technology, Harbin 150090, China (Corresponding author). Email: maxianyong@hit.edu.cn

[4]Professor, School of Transportation Science and Engineering, Harbin Institute of Technology, Harbin 150090, China. Email: hitclp@hit.edu.cn

[5]Professor, School of Highway, Chang'an University, Xi'an 710064, China. Email: zhliang0105@163.com

[6]Assistant Professor, Department of Civil and Environment Engineering, Hong Kong Polytechnic University, Hong Kong, PR China. E-mail: zhen.leng@polyu.edu.hk

Abstract: The conventional transfer matrix method, adopted formerly in a semi analytical solution for layered elastic or viscoelastic asphalt pavement system, has inherent deficiencies, such as ill-condition matrix, numerical overflow and error accumulation, due to exponential items. This phenomenon is more evident in multilayered dynamic analysis with imperfect interfaces. Moreover, several studies revealed that pavement materials exhibit transverse isotropy in service. Consequently, a novel semi analytical solution methodology, wave propagation approach, was proposed herein to calculate the dynamic responses of asphalt pavement under an impact load considering the transversely isotropic material model and the imperfect interfaces. First, the transfer matrix was established based on matrix theory and wave propagation approach, while the relation between the state vector and wave vector in the transformed domain was constructed simultaneously. Then, combined with the boundary conditions and interface contact conditions, the solution of the wave vector in the transformed domain was derived. Finally, based on Laplace–Hankel inverse transform, the state vector in the time domain was obtained, followed by numerical computation with programming. The accuracy and efficiency of the proposed semi analytical solution, together with the influence regularities of several variables, were discussed. Results showed that due to the absence of positive exponential functions and a large-dimensional matrix, accuracy and efficiency requirements were satisfied during calculation. Moreover, the variation induced by the transversely isotropic properties and interface conditions, presented in the dynamic responses, reiterated that these factors should be considered during the design and analysis of asphalt pavement structures.

Author keywords: asphalt pavement, impact load, dynamic responses, wave propagation approach, transversely isotropic

1. Introduction

Asphalt pavement is a layered structure in nature. As a convenient, efficient tool in pavement analysis and design, semi analytical solutions for the multilayer structure have been accepted by pavement engineers worldwide (Maina and Matsui 2005; Erlingsson and Ahmed 2013; Khazanovich and Wang 2007). Over the past decades, the transfer matrix method (TMM) was widely utilized in the semi analytical solution of layered structures due to its clear concept and high efficiency (Hanskell 1953; Dong and Ma 2018). However, it may fail in the analysis of the layered structure with many imperfect interfaces (Cai and Pan 2018). An overflow could occur if the integral variable is very large, or the layer thickness is large (Pan 2019). This phenomenon is more evident when conducting dynamic analysis of the multilayered structure (Liu et al. 2018; Zhang and Gao 2019). Several scholars (Ai et al. 2017; Liu and Pan 2018; Zhang and Pan 2020) modified the constant coefficients in the general solutions of the layered structure to avoid positive exponential functions and adopted the dual variable and position method to maintain numerical stability during calculation and solve this problem. Special treatments of positive exponential functions can also be found in other matrix methods such as the compound matrix method (Dukin 1965; Schwab and Knopoff 1970), the exact stiffness matrix method (Senjuntichai and Rajapakse 1995; Mesgouez and Lefeuve-Mesgouez 2009), the backward TMM (Yue and Yin 1995), the orthogonalization method (Wang 1999), the spectral element method (Al-Khoury et al. 2001; You et al. 2018), and the analytical layer-element method (Yan et al. 2016; Ai et al. 2014). Another semi analytical method, named precise integration method, utilized Taylor expansion to calculate the exponential matrix function; thus, it can also avoid overflow in calculation (Zhong et al. 2004; Lin et al. 2013; Ai et al. 2014).

In the above matrix methods with desirable stability, the exact stiffness matrix method, spectral element method, and analytical layer-elemen method have been applied in pavement engineering (Zhong et al. 2003; You et al. 2018; Yan et al. 2016). What these methods have in common is that they combine multilayered elastic theory with the concept of global stiffness matrix in the finite element method (FEM) and deem the displacements of each layer as the undetermined parameters. The accuracy of these methods is desirable due to the absence of positive exponential functions. However, with the increase of the layer number, the larger global matrix will have a negative effect on calculation efficiency (Blum 2012). As one of the numerically stable methods without disturbance from positive exponential functions, the wave propagation approach was first proposed by Luco (1983). Initially, this approach was adopted to investigate the wave propagation caused by earthquake load in soil (Apsel and Luco 1983). Pak adopted this approach in the derivation of Green’s function for layered soil under point load (Pak and Guzina 2002). Unlike the analysis in soil, more layers and unique loading type were included in pavement analysis (Dong and Ma 2018; Liu et al. 2018; Cai et al. 2015). Moreover, the TMM has been widely used in pavement engineering. Therefore, using wave propagation approach to reconstruct the transfer matrix and obtaining the responses in asphalt pavement are meaningful.

In addition, scholars found that road materials (asphalt concrete, base layers, and soil) in the pavement exhibit anisotropic properties due to natural deposition and compaction (Papadopoulos and Santamarina 2016; Al-Qadi et al. 2010; Ahmed et al. 2013). The anisotropic properties of materials could be approximated as transverse isotropy to simplify the calculation procedures and reveal the influence of anisotropic properties on the responses of asphalt pavement (You et al. 2019). Transverse isotropy means that the modulus is the same in one plane (horizontal plane) and different in the direction perpendicular to the plane (vertical direction). Based on measured data, the influences of transverse isotropy of pavement materials on the responses of pavement structure have been investigated using the FEM. Wang et al. (2005) found that the horizontal modulus to vertical modulus of asphalt mixture is in the range of 0.2–0.5, and the isotropic model would underestimate the tensile stress and shear stress of the asphalt layer. Tutumluer et al. (1997) found that the horizontal modulus of granular materials is about 3%–21% of the vertical modulus and introduced the transverse isotropic constitutive model to the granular base to eliminate or reduce the tensile stress concentration phenomenon caused by the isotropic model. Semi analytical solutions for transversely isotropic asphalt pavement have focused on static analysis (Liu et al. 2018; Ai et al. 2014; Cai et al. 2015; Ernian 1989), while a few solutions have been proposed for the analysis of the dynamic responses of asphalt pavement under transient load (You et al. 2018; Yan et al. 2016). As an important factor of pavement service life (Kruntcheva et al. 2015; Mousa et al. 2019; Liu and Pan 2018), interface bonding condition was not considered in the above transient semi analytical solutions for asphalt pavement. Therefore, a transient, dynamic, semi analytical solution that can consider the transverse isotropy of the material and the imperfect interface between different layers must be established.

The objective of this paper is to develop an efficient, accurate, semi analytical solution for transversely isotropic asphalt pavement under an impact load. Detailed mathematical derivations for applying wave propagation approach in the reconstruction of transfer matrix are provided. A program for the numerical results of the proposed semi analytical solution is compiled, and its accuracy and efficiency are then validated. In addition, the influences of interface bonding conditions and transverse isotropy of structure layers on the dynamic responses of asphalt pavement are discussed.

2 Governing Differential Equations for Elastic Media

2.1 Equilibrium Equations

Herein, the axisymmetric layered elastic system subjected to a uniform circular impact loading is investigated. As a result, the cylindrical coordinate system (r, θ, z) is employed to obtain the semi analytical solution for the dynamic responses of pavement structure. The origin of this coordinate system is set on the surface of pavement structure, and z-axis is the symmetric axle of the system. ρ and c_{ij} are the density and elastic constants of the material, respectively. The equilibrium equation can be written as

$$\frac{\partial \sigma_r}{\partial r} + \frac{\partial \tau_{zr}}{\partial z} + \frac{\sigma_r - \sigma_\theta}{r} = \rho \frac{\partial^2 u}{\partial t^2} \tag{1a}$$

$$\frac{\partial \tau_{zr}}{\partial r} + \frac{\partial \sigma_z}{\partial z} + \frac{\tau_{zr}}{r} = \rho \frac{\partial^2 w}{\partial t^2} \tag{1b}$$

where σ_r , σ_θ , and σ_z are the normal stress variables along coordinate axes *r*, *θ*, and *z*, respectively; τ_{zr} is the shear stress in plane *z*-*r*; *u* and *w* are the displacements in the *r* and *z* directions, respectively; and *t* is time.

2.2 Physical Equations

The physical equations for transversely isotropic material can be written as:

$$\begin{bmatrix} \sigma_r(r,z,t) \\ \sigma_\theta(r,z,t) \\ \sigma_z(r,z,t) \\ \tau_{zr}(r,z,t) \end{bmatrix} = \begin{bmatrix} c_{11} & c_{12} & c_{13} & 0 \\ c_{12} & c_{11} & c_{13} & 0 \\ c_{13} & c_{13} & c_{33} & 0 \\ 0 & 0 & 0 & c_{44} \end{bmatrix} \begin{bmatrix} \varepsilon_r(r,z,t) \\ \varepsilon_\theta(r,z,t) \\ \varepsilon_z(r,z,t) \\ \gamma_{zr}(r,z,t) \end{bmatrix} \tag{2}$$

where ε_r , ε_θ , and ε_z are the normal strains corresponding to stresses σ_r , σ_θ , and σ_z , respectively; γ_{zr} is the shear strain corresponding to shear stress τ_{zr} ; and c_{ij} are elastic constants.

Elastic constants c_{ij} could be presented by material parameters as follows:

$$c_{11} = \frac{-E_v k_1 (k_1 \mu_v{}^2 - 1)}{\mu_h{}^2 + 2k_1 \mu_h \mu_v{}^2 + 2k_1 \mu_v{}^2 - 1} \tag{3a}$$

$$c_{12} = \frac{-E_v k_1 (k_1 \mu_v{}^2 + \mu_h)}{\mu_h{}^2 + 2k_1 \mu_h \mu_v{}^2 + 2k_1 \mu_v{}^2 - 1} \tag{3b}$$

$$c_{13} = \frac{-E_v \mu_v k_1}{2k_1 \mu_v{}^2 + \mu_h - 1} \tag{3c}$$

$$c_{33} = \frac{E_v (\mu_h - 1)}{2k_1 \mu_v{}^2 + \mu_h - 1} \tag{3d}$$

$$c_{44} = k_2 E_v \tag{3e}$$

$$k_1 = E_h / E_v \tag{3f}$$

$$k_2 = G_v / E_v \tag{3g}$$

where E_v and E_h are the Young's moduli in the vertical and horizontal directions, respectively; G_v is the shear modulus in planes normal to the plane of transverse isotropy; μ_h and μ_v are Poisson's ratios in the horizontal and vertical directions, respectively; and k_1 and k_2 are the ratios between moduli.

2.3 Geometric Equations

The relations between strains and displacements in an axisymmetric system are as follows:

$$\varepsilon_r = \frac{\partial u}{\partial r} \tag{4a}$$

$$\varepsilon_\theta = \frac{u}{r} \tag{4b}$$

$$\varepsilon_z = \frac{\partial w}{\partial z} \tag{4c}$$

$$\gamma_{zr} = \frac{\partial u}{\partial z} + \frac{\partial w}{\partial r} \tag{4d}$$

3 Single-Layered Wave Vector for Elastic Media

A state vector is first derived based on the TMM. Then, it is converted into a wave vector based on the wave propagation approach to ensure numerical stability.

3.1 State Vector

Based on the TMM, the partial differential equations shown in Eqs. (1), (2), and (4) can be rewritten to construct a state vector. When selecting w, u, σ_z, and τ_{zr} as the component of the state vector, the following equations can be obtained:

$$\frac{\partial w}{\partial z} = c_3\sigma_z + c_2\frac{u}{r} + c_2\frac{\partial u}{\partial r} \tag{5a}$$

$$\frac{\partial u}{\partial z} = c_1\tau_{zr} - \frac{\partial w}{\partial r} \tag{5b}$$

$$\frac{\partial \sigma_z}{\partial z} = \rho\frac{\partial w^2}{\partial t^2} - \frac{\tau_{zr}}{r} - \frac{\partial \tau_{zr}}{\partial r} \tag{5c}$$

$$\frac{\partial \tau_{zr}}{\partial z} = -c_4\left(\frac{\partial u^2}{\partial r^2} + \frac{1}{r}\frac{\partial u}{\partial r} - \frac{u}{r^2}\right) + c_2\frac{\partial \sigma_z}{\partial r} + \rho\frac{\partial u^2}{\partial t^2} \tag{5d}$$

where $c_1 = \dfrac{1}{c_{44}}$, $c_2 = -\dfrac{c_{13}}{c_{33}}$, $c_3 = \dfrac{1}{c_{33}}$, $c_4 = c_{11} - \dfrac{c^2{}_{13}}{c_{33}}$, and $c_5 = c_{12} - \dfrac{c^2{}_{13}}{c_{33}}$.

Applying Laplace transform on the time and Hankel transform on the radial coordinate, Laplace transform and its inverse form are:

$$\bar{f}(s) = \int_0^\infty f(t)e^{-st}dt \tag{6a}$$

$$f(t) = \frac{1}{2\pi i}\int_{a-i\infty}^{a+i\infty} \bar{f}(s)e^{st}ds \tag{6b}$$

The mth-order Hankel and its inverse transform are defined as:

$$\hat{f}^m(\xi) = \int_0^\infty rf(r)J_m(r\xi)dr \tag{7a}$$

$$f(r) = \int_0^\infty \xi \hat{f}(\xi)J_m(r\xi)d\xi \tag{7b}$$

Applying zeroth-order Hankel transform and Laplace transform into Eqs. (5a) and (5c) while applying first-order Hankel transform and Laplace transform into Eqs. (5b) and (5d) can obtain that

$$\frac{d[\hat{\hat{\mathbf{X}}}]}{dz} = [\hat{\hat{\mathbf{A}}}(\xi, s)][\hat{\hat{\mathbf{X}}}] \tag{8a}$$

$$[\hat{\hat{\mathbf{A}}}]_{4\times4} = \begin{bmatrix} 0 & \xi & 0 & c_1 \\ c_2\xi & 0 & c_3 & 0 \\ 0 & \rho s^2 & 0 & -\xi \\ c_4\xi^2 + \rho s^2 & 0 & -c_2\xi & 0 \end{bmatrix} \tag{8b}$$

$$\begin{aligned} [\hat{\hat{\mathbf{X}}}]_{4\times1} &= \int_0^\infty \int_0^\infty [uJ_1(\xi r) \quad wJ_0(\xi r) \quad \sigma_z J_0(\xi r) \quad \tau_{zr} J_1(\xi r)]^T re^{-st}drdt \\ &= \left[\hat{\bar{u}}^{[1]} \quad \hat{\bar{w}}^{[0]} \quad \hat{\bar{\sigma}}_{\mathbf{z}}{}^{[0]} \quad \hat{\bar{\tau}}_{zr}{}^{[1]}\right]^T \end{aligned} \tag{8c}$$

According to theory of matrix differential equations, the solution of Eq. (8) is:

$$\hat{\hat{\mathbf{X}}} = \mathbf{e}^{\hat{\hat{\mathbf{A}}}(\xi,s)z}\hat{\hat{\mathbf{X}}}_0(\xi, s, 0) \tag{9}$$

where $\hat{\hat{\mathbf{X}}}_0(\xi, s, 0)$ is the initial state vector in the transformed domain, and $\mathbf{e}^{\hat{\hat{\mathbf{A}}}(\xi,s)z}$ is the exponential function of matrix $\hat{\hat{\mathbf{A}}}$.

3.2 Wave Vector from State Vector

The state vector at any depth of a single layer can be derived via Eq. (9). Furthermore, the characteristic equation of matrix $\hat{\hat{\mathbf{A}}}$ is:

$$\lambda^4 + \delta_1 \lambda^2 + \delta_0 = 0 \tag{10}$$

where $\delta_1 = -(2c_2 + c_1 c_4)\xi^2 - \rho s^2 (c_1 + c_3)$, and $\delta_0 = (\xi^2 + c_1 \rho s^2)(c_2{}^2 \xi^2 + c_3 c_4 \xi^2 + c_3 \rho s^2)$.

The roots of Eq. (10) are:

$$\lambda_1 = -\sqrt{\frac{-\delta_1 + \sqrt{\delta_1{}^2 - 4\delta_0}}{2}} \tag{11a}$$

$$\lambda_2 = -\sqrt{\frac{-\delta_1 - \sqrt{\delta_1{}^2 - 4\delta_0}}{2}} \tag{11b}$$

$$\lambda_3 = -\lambda_1 \tag{11c}$$

$$\lambda_4 = -\lambda_2 \tag{11d}$$

Consequently, $\mathbf{e}^{\hat{\bar{\mathbf{A}}}(\xi,s)z}$ can be expressed as:

$$\mathbf{e}^{\hat{\bar{\mathbf{A}}}(\xi,s)z} = [\mathbf{P}]_{4\times4}[diag(e^{\lambda_1 z}, e^{\lambda_2 z}, e^{\lambda_3 z}, e^{\lambda_4 z})]_{4\times4}[\mathbf{P}^{-1}]_{4\times4} \tag{12}$$

where $diag$ is the symbol of diagonal matrix, $\mathbf{P}$ is a matrix whose columns are the corresponding eigenvectors of $\hat{\bar{\mathbf{A}}}(\xi,s)$, and $\mathbf{P}^{-1}$ is the inverse matrix of $\mathbf{P}$.

In the conventional TMM, relationships of state vectors between the top surface and any point within the layer could be established based on Eqs. (9) and (12). However, Eq. (12) shows that the matrix involved in the TMM contains several positive exponential functions, thus causing computational overflow and accuracy loss. The wave propagation approach is adopted here to solve these problems. Relationships between the state vectors are transformed into those between wave vectors by constructing the wave vector. Therefore, the positive exponential functions in the original matrix function ($\mathbf{e}^{\hat{\bar{\mathbf{A}}}(\xi,s)z}$) can be eliminated in the following derivation. According to matrix multiplication law, substituting Eq. (12) into Eq. (9) yields:

$$\hat{\bar{\mathbf{X}}} = [\mathbf{l}_1, \mathbf{l}_2, \mathbf{l}_3, \mathbf{l}_4]_{4\times4}[diag(e^{\lambda_1 z}, e^{\lambda_2 z}, e^{\lambda_3 z}, e^{\lambda_4 z})]_{4\times4}[x_1 \quad x_2 \quad x_3 \quad x_4]^T{}_{4\times1} = \sum_{i=1}^{4} x_i e^{\lambda_i z}[\mathbf{l}_i]_{4\times1}, \tag{13a}$$

$$[x_1 \quad x_2 \quad x_3 \quad x_4]^T = \mathbf{P}^{-1}\hat{\bar{\mathbf{X}}}_0(\xi, s, 0) \tag{13b}$$

where $\mathbf{l}_i$ is the column vector of $\mathbf{P}$.

Eq. (11) is substituted into Eq. (13) to construct the upgoing wave vector and the downgoing wave vector, and the following equation can be obtained:

$$\hat{\hat{\mathbf{X}}}=\begin{bmatrix} l_1^{(1)} & l_2^{(1)} & l_3^{(1)} & l_4^{(1)} \\ l_1^{(2)} & l_2^{(2)} & l_3^{(2)} & l_4^{(2)} \\ l_1^{(3)} & l_2^{(3)} & l_3^{(3)} & l_4^{(3)} \\ l_1^{(4)} & l_2^{(4)} & l_3^{(4)} & l_4^{(4)} \end{bmatrix}\begin{bmatrix} x_1e^{\lambda_1 z} \\ x_2e^{\lambda_2 z} \\ x_3e^{-\lambda_1 z} \\ x_4e^{-\lambda_2 z} \end{bmatrix} \tag{14}$$

where $l_i^{(j)}$ represents the *j*th element of the *i*th column vector within matrix $\mathbf{P}$.

Based on the principle of wave propagation approach and matrix partitioning, the negative exponential functions in $\hat{\hat{\mathbf{X}}}$ constitute the downgoing wave matrix, and the positive exponential functions in $\hat{\hat{\mathbf{X}}}$ constitute the upgoing wave matrix. Based on Eq. (14), the relationship between the state vector $\hat{\hat{\mathbf{X}}}$ and the wave vector $[\mathbf{W}]_{4\times1}$ is:

$$\hat{\hat{\mathbf{X}}}(\xi,s,z)=[\mathbf{M}(\xi,s)]_{4\times4}[\mathbf{W}(\xi,s,z)]_{4\times1} \tag{15a}$$

$$[\mathbf{M}(\xi,s)]_{4\times4}=\begin{bmatrix} l_1^{(1)} & l_2^{(1)} & l_3^{(1)} & l_4^{(1)} \\ l_1^{(2)} & l_2^{(2)} & l_3^{(2)} & l_4^{(2)} \\ l_1^{(3)} & l_2^{(3)} & l_3^{(3)} & l_4^{(3)} \\ l_1^{(4)} & l_2^{(4)} & l_3^{(4)} & l_4^{(4)} \end{bmatrix}=\begin{bmatrix} [\mathbf{D}_d(\xi,s)]_{2\times2} & [\mathbf{D}_u(\xi,s)]_{2\times2} \\ [\mathbf{S}_d(\xi,s)]_{2\times2} & [\mathbf{S}_u(\xi,s)]_{2\times2} \end{bmatrix} \tag{15b}$$

$$[\mathbf{W}(\xi,s,z)]_{4\times1}=[[\mathbf{W}_d(\xi,s,z)]_{2\times1}{}^T,[\mathbf{W}_u(\xi,s,z)]_{2\times1}{}^T]^T \tag{15c}$$

$$[\mathbf{W}_d(\xi,s,z)]_{2\times1}=\begin{bmatrix} x_1e^{\lambda_1 z} & x_2e^{\lambda_2 z} \end{bmatrix}^T \tag{15d}$$

$$[\mathbf{W}_u(\xi,s,z)]_{2\times1}=\begin{bmatrix} x_3e^{-\lambda_1 z} & x_4e^{-\lambda_2 z} \end{bmatrix}^T \tag{15e}$$

where subscripts *d* and *u* represent the block matrix related to the downgoing and upgoing wave, respectively; $\mathbf{D}_d(\xi,s)$, $\mathbf{D}_u(\xi,s)$, $\mathbf{S}_d(\xi,s)$, and $\mathbf{S}_u(\xi,s)$ are the block matrixes of transform matrix $\mathbf{M}(\xi,s)$; and $\mathbf{W}_d(\xi,s,z)$ and $\mathbf{W}_u(\xi,s,z)$ are the downgoing and upgoing wave vectors, respectively.

A scheme is adopted by this paper to deal with the positive exponential and eliminate it during calculation. For the single-layered system shown in Fig. 1, the undetermined coefficients named x_1, x_2, x_3, and x_4 can be replaced by a, b, $ce^{\lambda_1 h}$, and $de^{\lambda_2 h}$ separately. Consequently, the following equations can be obtained:

$$\mathbf{W}_d(\xi,s,z)=\begin{bmatrix} ae^{\lambda_1 z} & be^{\lambda_2 z} \end{bmatrix}^T \tag{16a}$$

$$\mathbf{W}_u(\xi,s,z)=\left[ce^{\lambda_1(h-z)} \quad de^{\lambda_2(h-z)}\right]^T \tag{16b}$$

Based on Eq. (16), the downgoing and upgoing wave vectors at any depth ($0\le z\le h$) of the layer are:

$$\mathbf{W}_d(\xi,s,z)=[\mathbf{E}(z)]_{2\times2}\mathbf{W}_d(\xi,s,0) \tag{17a}$$

$$\mathbf{W}_u(\xi,s,z)=[\mathbf{E}(h-z)]_{2\times2}\mathbf{W}_u(\xi,s,h) \tag{17b}$$

where $\mathbf{E}(\chi)=\begin{bmatrix} e^{\lambda_1\chi} & 0 \\ 0 & e^{\lambda_2\chi}\end{bmatrix}$.

Eq. (17) shows that in the transformed domain, if the wave vectors at the bottom and top of the layer are obtained, then the wave vector at any depth of the layer can be derived. Moreover, based on Eq. (15), the state vector in the transformed domain can be calculated subsequently. The following recursive relationship between wave vectors derived from Eq. (17) is numerically stable because only negative exponential terms are involved.

4 Solution of Multilayered Elastic Structures

The wave and state vector at any depth in one specific layer in a multilayered structure can be calculated from the wave vectors at the bottom and top of the layer. In this section, based on the interface bonding conditions and boundary conditions, the wave and state vectors in the transformed domain at any depth are derived. Then, the numerical solution for dynamic responses in the time domain utilizing the Hankel and Laplace inverse transforms are provided.

4.1 Wave and State Vectors at Any Depth in Transformed Domain

Based on the wave vector, the dynamic responses of a multilayered elastic structure (shown in Fig. 1) subjected to an impact loading are solved in this section. The Goodman model is adopted to describe the continuous, sliding, and semi contact conditions between layers (Kruntcheva et al. 2005; Mousa et al. 2019). The value of the spring stiffness in the Goodman model can be obtained from indoor experiments or back-calculation based on field tests (Yue and Yin 1998; Mousa et al. 2019). Therefore, the relationship of state vectors between layers is:

$$\begin{bmatrix} 1 & 0 & 0 & 1/k_r^j \\ 0 & 1 & 0 & 0 \\ 0 & 0 & 1 & 0 \\ 0 & 0 & 0 & 1 \end{bmatrix} \hat{\hat{\mathbf{X}}}^j(\xi, s, z_j) = \hat{\hat{\mathbf{X}}}^{j+1}(\xi, s, z_j) \tag{18}$$

where z_j presents the coordinates at the bottom of the *j*th layer, k_r^j is the spring stiffness between the *j*th and (*j*+1) th layer, $\hat{\hat{\mathbf{X}}}^j(\xi, s, z_j)$ is the state vector at the bottom of the *j*th layer, and $\hat{\hat{\mathbf{X}}}^{j+1}(\xi, s, z_j)$ is the state vector at the top of the (*j*+1)th layer.

Based on Eq. (15), Eq. (18) can be rewritten in matrix form as follows:

$$\begin{bmatrix} \mathbf{W}_d^{j+1}(\xi, s, z_j) \\ \mathbf{W}_u^j(\xi, s, z_j) \end{bmatrix}_{4\times 1} = \begin{bmatrix} \mathbf{T}_d^j(\xi, s) & \mathbf{R}_u^j(\xi, s) \\ \mathbf{R}_d^j(\xi, s) & \mathbf{T}_u^j(\xi, s) \end{bmatrix}_{4\times 4} \begin{bmatrix} \mathbf{W}_d^j(\xi, s, z_j) \\ \mathbf{W}_u^{j+1}(\xi, s, z_j) \end{bmatrix}_{4\times 1} \tag{19a}$$

$$\begin{bmatrix} \mathbf{T}_d^j(\xi, s) & \mathbf{R}_u^j(\xi, s) \\ \mathbf{R}_d^j(\xi, s) & \mathbf{T}_u^j(\xi, s) \end{bmatrix}_{4\times 4} = \begin{bmatrix} -\mathbf{D}_d^{j+1}(\xi, s) & \mathbf{D}_{um}^j(\xi, s) \\ -\mathbf{S}_d^{j+1}(\xi, s) & \mathbf{S}_u^j(\xi, s) \end{bmatrix}_{4\times 4}^{-1} \begin{bmatrix} -\mathbf{D}_{dm}^j(\xi, s) & \mathbf{D}_u^{j+1}(\xi, s) \\ -\mathbf{S}_d^j(\xi, s) & \mathbf{S}_u^{j+1}(\xi, s) \end{bmatrix}_{4\times 4} \tag{19b}$$

$$[\mathbf{D}_{um}^j(\xi, s)]_{2\times 2} = [\mathbf{D}_u^j(\xi, s)]_{2\times 2} + [\mathbf{S}_u^j(\xi, s)]_{2\times 2} \begin{bmatrix} 0 & 1/k_r^j \\ 0 & 0 \end{bmatrix} \tag{19c}$$

$$[\mathbf{D}_{dm}^j(\xi, s)]_{2\times 2} = [\mathbf{D}_d^j(\xi, s)]_{2\times 2} + [\mathbf{S}_d^j(\xi, s)]_{2\times 2} \begin{bmatrix} 0 & 1/k_r^j \\ 0 & 0 \end{bmatrix} \tag{19d}$$

where $[\mathbf{R}_u^j(\xi, s)]_{2\times 2}$ and $[\mathbf{R}_d^j(\xi, s)]_{2\times 2}$ are the reflection and transmission matrixes of P wave, respectively; and $[\mathbf{T}_u^j(\xi, s)]_{2\times 2}$ and $[\mathbf{T}_d^j(\xi, s)]_{2\times 2}$ are the reflection and transmission matrixes of S wave, respectively.

Substituting $j = n$ into Eq. (19a), the wave vectors in *n*th and (*n*+1)th layers can be obtained:

$$\mathbf{W}_d^{n+1}(\xi, s, z_n) = \mathbf{T}_d^n(\xi, s)\mathbf{W}_d^n(\xi, s, z_n) + \mathbf{R}_u^n(\xi, s)\mathbf{W}_u^{n+1}(\xi, s, z_n) \tag{20a}$$

$$\mathbf{W}_u^n(\xi, s, z_n) = \mathbf{R}_d^n(\xi, s)\mathbf{W}_d^n(\xi, s, z_n) + \mathbf{T}_u^n(\xi, s)\mathbf{W}_u^{n+1}(\xi, s, z_n) \tag{20b}$$

The following can be known from the reference (Caviglia and Morro 2000):

$$\mathbf{W}_u^{n+1}(\xi, s, z_n) = \mathbf{0} \tag{21}$$

Substituting Eq. (21) into Eq. (20), the wave vectors in *n*th and (*n*+1)th layers can be simplified as:

$$\mathbf{W}_d^{n+1}(\xi, s, z_n) = \mathbf{T}_d^{gn}(\xi, s)\mathbf{W}_d^n(\xi, s, z_n) \tag{22a}$$

$$\mathbf{W}_u^n(\xi,s,z_n)=\mathbf{R}_d^{gn}(\xi,s)\mathbf{W}_d^n(\xi,s,z_n) \tag{22b}$$

where $[\mathbf{T}_d^{gn}(\xi,s)]_{2\times2}=\mathbf{T}_d^n(\xi,s)$, and $[\mathbf{R}_d^{gn}(\xi,s)]_{2\times2}=[\mathbf{R}_d^n(\xi,s)]_{2\times2}$.

Substituting $j=n-1$ into Eq. (19a) to obtain the recursive relationship of wave vectors in jth layer yields

$$\mathbf{W}_d^n(\xi,s,z_{n-1})=\mathbf{T}_d^{n-1}(\xi,s)\mathbf{W}_d^{n-1}(\xi,s,z_{n-1})+\mathbf{R}_u^{n-1}(\xi,s)\mathbf{W}_u^n(\xi,s,z_{n-1}) \tag{23a}$$

$$\mathbf{W}_u^{n-1}(\xi,s,z_{n-1})=\mathbf{R}_d^{n-1}(\xi,s)\mathbf{W}_d^{n-1}(\xi,s,z_{n-1})+\mathbf{T}_u^{n-1}(\xi,s)\mathbf{W}_u^n(\xi,s,z_{n-1}) \tag{23b}$$

Based on Eqs. (23b) and (17), the following can be given:

$$\mathbf{W}_u^n(\xi,s,z_{n-1})=\mathbf{E}^n(h_n)\mathbf{R}_d^{gn}(\xi,s)\mathbf{E}^n(h_n)\mathbf{W}_d^n(\xi,s,z_{n-1}) \tag{24}$$

Substituting Eq. (24) into Eq. (23a) yields:

$$\mathbf{W}_d^n(\xi,s,z_{n-1})=\mathbf{T}_{de}^{g(n-1)}(\xi,s)\mathbf{W}_d^{n-1}(\xi,s,z_{n-2}) \tag{25a}$$

$$[\mathbf{T}_{de}^{g(n-1)}(\xi,s)]_{2\times2}=[\mathbf{I}-\mathbf{R}_u^{n-1}(\xi,s)\mathbf{E}^n(h_n)\mathbf{R}_d^{gn}(\xi,s)\mathbf{E}^n(h_n)]^{-1}\mathbf{T}_d^{n-1}(\xi,s)\mathbf{E}^{n-1}(h_{n-1}) \tag{25b}$$

where $[\mathbf{I}]_{2\times2}$ represents the identity matrix.

Based on Eqs. (22a) and (25a), the recursive relations of the downgoing vectors between layers are:

$$\mathbf{W}_d^j(\xi,s,z_{j-1})=\mathbf{T}_{de}^{g(j-1)}(\xi,s)\mathbf{T}_{de}^{g(j-2)}(\xi,s)...\mathbf{T}_{de}^{g1}(\xi,s)\mathbf{W}_d^1(\xi,s,z_0)\quad j=1,2,\cdots n \tag{26a}$$

$$\mathbf{W}_d^j(\xi,s,z_{j-1})=\mathbf{T}_{de}^{j\text{-}1}(\xi,s)\mathbf{E}^j(h_j)\mathbf{W}_d^{j-1}(\xi,s,z_{j-2})\quad j=n+1 \tag{26b}$$

$$[\mathbf{T}_{de}^{g(j-1)}(\xi,s)]_{2\times2}=[\mathbf{I}-\mathbf{R}_u^{j\text{-}1}(\xi,s)\mathbf{E}^j(h_j)\mathbf{R}_d^{gj}(\xi,s)\mathbf{E}^j(h_j)]^{-1}\mathbf{T}_d^{j-1}(\xi,s)\mathbf{E}^{j-1}(h_{j-1}) \tag{26c}$$

Substituting Eq. (24) into Eq. (23b) yields:

$$\mathbf{W}_u^{n-1}(\xi,s,z_{n-1})=\mathbf{R}_d^{n-1}(\xi,s)\mathbf{W}_d^{n-1}(\xi,s,z_{n-1})+\mathbf{T}_u^{n-1}(\xi,s)\mathbf{E}^n(h_n)\mathbf{R}_{de}^{gn}(\xi,s)\mathbf{W}_d^n(\xi,s,z_{n-1}), \tag{27}$$

where $[\mathbf{R}_{de}^{gn}(\xi,s)]_{2\times2}=\mathbf{R}_d^{gn}(\xi,s)\mathbf{E}^n(h_n)$.

Substituting Eq. (25a) into Eq. (27) yields:

$$\mathbf{W}_u^{n-1}(\xi,s,z_{n-1})=\mathbf{R}_{de}^{g(n-1)}(\xi,s)\mathbf{W}_d^{n-1}(\xi,s,z_{n-2}) \tag{28a}$$

$$[\mathbf{R}_{de}^{g(n-1)}(\xi,s)]_{2\times2}=[\mathbf{R}_d^{n-1}(\xi,s)+\mathbf{T}_u^{n-1}(\xi,s)\mathbf{E}^n(h_n)\mathbf{R}_{de}^{gn}(\xi,s)\mathbf{T}_d^{g(n-1)}(\xi,s)]\mathbf{E}^{n-1}(h_{n-1}) \tag{28b}$$

Based on Eqs. (23b) and (28a), the recursive relations of the upgoing vectors between layers are:

$$\mathbf{W}_u^j(\xi,s,z_j)=\mathbf{R}_{de}^{gj}(\xi,s)\mathbf{W}_d^j(\xi,s,z_{j\text{-}1})\quad j=1,2,\cdots n\text{-}1 \tag{29a}$$

$$\mathbf{W}_u^j(\xi,s,z_j)=\mathbf{R}_{d}^{gj}(\xi,s)\mathbf{E}^j(h_j)\mathbf{W}_d^j(\xi,s,z_{j\text{-}1})\quad j=n \tag{29b}$$

$$[\mathbf{R}_{de}^{g(j)}(\xi,s)]_{2\times 2}=[\mathbf{R}_d^j(\xi,s)+\mathbf{T}_u^j(\xi,s)\mathbf{E}^{j+1}(h_{j+1})\mathbf{R}_d^{g(j+1)}(\xi,s)\mathbf{E}^{j+1}(h_{j+1})\mathbf{T}_d^{gj}(\xi,s)]\mathbf{E}^j(h_j) \tag{29c}$$

Eqs. (17), (26), and (29) reveal that the upgoing and downgoing wave vectors at any depth in the transformed domain are dependent on the downgoing wave vector at the top of the first layer.

When the top surface of the multilayered pavement structure is subjected to impact loading as shown in Fig. 2, substituting $j=1$ and $z=z_0$ into Eq. (15) yields:

$$\mathbf{S}_d^1(\xi,s)\mathbf{W}_d^1(\xi,s,z_0)+\mathbf{S}_u^1(\xi,s)\mathbf{W}_u^1(\xi,s,z_0)=\hat{\bar{\mathbf{L}}}(\xi,s) \tag{30}$$

where $[\hat{\bar{\mathbf{L}}}(\xi,s)]_{2\times 1}=[-\hat{\bar{F}}(\xi,s)\quad 0]^T$.

The impact loading in the time domain can be expressed as:

$$F(r,t)=\begin{cases} V\sin(\dfrac{\pi t}{T_d}) & r\le R, 0\le t\le T_d \\ 0 & r>R, t>T_d \end{cases} \tag{31}$$

where V is the peak value of the uniformly distributed impact load, R is the radius of the impact load, and T_d is the duration of the impact load.

Applying Laplace and zeroth-order Hankel transform to Eq. (31) yields:

$$\hat{\bar{F}}(\xi,s)=\frac{\pi T_d(1+e^{-sT_d})}{s^2+\pi^2}\frac{VRJ_1(\xi R)}{\xi} \tag{32}$$

Based on Eqs. (15) and (30), the following equation can be obtained:

$$\mathbf{W}_d^1(\xi,s,z_0)=[\mathbf{S}_d^1(\xi,s)+\mathbf{S}_u^1(\xi,s)\mathbf{E}^1(h_1)\mathbf{R}_{de}^{g1}]^{-1}\hat{\bar{\mathbf{L}}}(\xi,s) \tag{33}$$

Based on Eqs. (15), (17), (26), (29), (32), and (33), the state vector at any depth in transformed domain can be obtained.

4.2 Numerical Solution Methodology

Numerical inverse transform schemes are adopted to obtain the wave vector in the time domain. Hankel and Laplace inverse transforms are carried out using segmented Gauss integral and Durbin approach, respectively. The realization of the numerical calculation of the semi analytical solution was compiled into a computer program. Taking the displacement as an example, the integral region is divided into g subintervals, and the inverse Hankel transform can be performed by using the following equation:

$$\bar{w}(r,s)=\int_0^\infty \hat{\bar{w}}(\xi,s)J_0(\xi r)\xi d\xi=\sum_{j=1}^{g}\int_{b_j}^{b_{j+1}}\hat{\bar{w}}(\xi,s)J_0(\xi r)\xi d\xi \tag{34}$$

where b_i is the zero point of zero-order Bessel function.

The first five circles in Eq. (34) are adopted to maintain calculation precision and efficiency. For each circle, a 32-node Gaussian approach is utilized. The validation section and the reference (Lee 2014) show that the proposed scheme is desirable. The *j*th integral interval can be calculated by the following equation:

$$\int_{b_j}^{b_{j+1}}\hat{\bar{w}}(\xi,s)J_0(\xi,r)\xi d\xi=\frac{b_{j+1}-b_j}{2}\sum_{i=1}^{32}A_i\hat{\bar{w}}(B_i,s)J_0(B_i,r)B_i \tag{35}$$

where $B_i=(\frac{b_{j+1}-b_j}{2})\alpha_i+(\frac{b_{j+1}+b_j}{2})$; and A_i and α_i are Gaussian nodes and their corresponding weights, respectively.

Similarly, taking the displacement as an example, the equation of the Durbin approach used in the inverse Laplace transform is as follows:

$$\begin{aligned} w(r,t)&=\frac{1}{2\pi i}\int_{a-i\infty}^{a+i\infty}\bar{w}(r,s)e^{st}ds=\frac{e^{\theta t}}{T}[\frac{1}{2}\mathrm{Re}(\bar{w}(r,\theta))+\\ &\sum_{k=1}^{m}\mathrm{Re}(\bar{w}(r,\theta+\frac{ik\pi}{T})\cos\frac{k\pi t}{T})-\sum_{k=1}^{m}\mathrm{Im}(\bar{w}(r,\theta+\frac{ik\pi}{T})\sin\frac{k\pi t}{T})] \end{aligned} \tag{36}$$

where θ, m, and T are coefficients according to the reference (Durbin 1974). In this paper, $\theta T=5$, $T=2T_c$, $m=50$, and T_c is the time span in analysis. The reference (Ai et al. 2017) and computational results in the verification section show that these values satisfy the accuracy requirement.

5 Results and Discussion

The computational accuracy and efficiency verification of the proposed semi analytical solution mentioned above is implemented herein. Then, the potential effect considering transverse isotropy and interface bonding on pavement mechanical analysis and structural design is explored to provide several hints for the future computational dynamics of asphalt pavement.

5.1 Computational Verification

5.1.1 Accuracy Verification

The accuracy of the proposed semi analytical solution is validated by comparing its numerical results with those of the existing semi analytical solutions and FEM jointly.

First, the proposed semi analytical solution is degenerated to an isotropic one with a continuous interface and further validated by the results from the reference based on the spectrum element method. Then, a 50 kN impact load with a duration of 25 ms and a radius of 150 mm is applied on a three-layered pavement. Other essential parameters and the results are shown in Fig. 3. Time histories of the surface deflections from the numerical results of the proposed semi analytical solution are almost identical to those from the reference (Al-Khoury et al. 2001).

Then, FEM based on Abaqus platform is adopted to validate the proposed semi analytical solution further. A symmetric multilayered pavement consisting of three layers presented in Table 1 is utilized here. Transverse isotropy is introduced in the base layer, while other layers are assumed isotropic. The interface condition between the asphalt and base layer is considered, whose spring stiffness is assumed as 10^5, 10^8, and 10^{11} N/m^3 separately.

In addition, a 49.5 kN impact load with a duration of 30 ms and a radius of 150 mm is applied to both models. The geometry of the FEM model extends to 10 m in the *x* and *z* directions, and the latter is used to represent the half-space foundation. The left side of the model is axisymmetric, while its bottom is fully fixed. An eight-node axisymmetric element is used in the mesh generation, whose sizes are smaller near the loading area to maintain FEM computational efficiency and accuracy. The FEM model after meshing is presented in Fig. 4.

Based on the calculation results of FEM and the proposed semi analytical solution, the time histories of the radial strains at the bottom of the surface layer under loading center and the vertical strains along the z direction under loading center at t = 0.018 are listed in Figs. 5 and 6, respectively. The results reveal that the accuracy of the proposed semi analytical solution is superior regardless of interface conditions.

5.1.2 Efficiency Verification

In this subsection, the efficiency of the numerical calculation program based on the proposed semi analytical solution is discussed by comparing its computational times under different cases. Moreover, the computational time of the proposed semi analytical solution is compared with that of the FEM. All the following cases are carried on an ordinary laptop, whose CPU is i5-8300H.

First, time histories of surface deflections of pavement structures with different numbers of layers and surface calculation points are obtained, and the computational time of each case is shown in Fig. 7. Increasing layer number only results in a linear increase in computational time because of the absence of the need for the assembly of a global stiffness matrix. The increase of layer number will not result in a dramatic reduction in computing efficiency when the wave propagation approach is adopted. Moreover, for the three-layered pavement structure, the efficiency of the numerical calculation of the proposed semi analytical solution (30 s for 3 calculation points) is higher than that of the other semi analytical solution in the reference published recently (180 s for 3 calculation points) (You et al. 2018), whose time consumption is six times longer than the presented one.

Subsequently, using the same computer, several pavement structures with different calculation points shown in Fig. 8 are adopted to compare the efficiency of the proposed semi analytical solution with that of the FEM. Fig. 9 shows that the efficiency of the proposed semi analytical solution is superior to that of the FEM when analyzing conventional pavement structure (less than six layers). Moreover, the modeling in the FEM is complicated, and the established 2D axisymmetric FEM model is not suitable for the non-axisymmetric analysis, such as the case of load superimposition. Furthermore, its coding is more convenient to be integrated into current pavement design program. Therefore, the proposed semi analytical solution is promising for the future development of structural design for transversely isotropic asphalt pavement.

5.2 Influences of Interface Bonding Condition on Dynamic Responses

The reference (Kruntcheva et al. 2005) based on the analysis of pavement structure under a static load indicated that the assumption of completely bonded condition between layers will overestimate the service life of pavement. In this paper, different interface contact conditions are interpreted by spring stiffness (k_r). Therefore, k_r is an important mechanical index for pavement design and accurate evaluation of the residual life of a pavement structure. Theoretically, when the magnitude of spring stiffness varies from 0 to infinity, the contact condition between layers changes from smooth to continuous. However, the spring stiffness magnitude of interface should have a sensitivity range that is greater than 0 and less than infinity in numerical calculations. The three-layered pavement structure presented in Table 1 is continuously analyzed in the following discussion to investigate the influence of interface bonding conditions on the dynamic responses of asphalt pavement and obtain the sensitivity range of the spring stiffness in dynamic analysis.

Fig. 10 presents the surface deflections at different radius positions with changing interface spring stiffnesses when t = 0.018 s. Surface deflection increases with the decreasing spring stiffness near the loading center. As the position becomes far from the loading center (such as r = 1.5 m), the spring stiffness has no effect on the surface deflection at all. When the interfacial spring stiffness varies from 10^{13} N/m^3 to 10^5 N/m^3, the surface deflection at the loading center (i.e., r = 0.0 m) rises by about 43.8%.

Fig. 11 shows the radial strains of the surface layer bottom at different radius positions with changing interface spring stiffness when t = 0.016 s. A similar trend can be observed regarding radial strain as the spring stiffness decreases. However, the maximum increasing magnitude of the radial strain caused by the interfacial spring stiffness is much higher than that of the surface deflections. The maximum value of the radial strain at the loading center is nearly 1.69 times that of the smallest one.

The 3D surfaces of radial strains when t = 0.016 s are drawn in Fig. 12, whose stiffness values are 10^6 and 10^{12} N/m^3 to understand the influence of interfacial spring stiffness on radial strains better. A smaller value of interfacial spring stiffness will result in a discontinuity of the radial strain between layers and a higher tensile strain at the bottom of the asphalt layer under the loading center. The interface condition should not be neglected during pavement mechanic analysis and structural design because the radial strain has a great influence on the fatigue life of asphalt pavement. In addition, the sensitivity range of interfacial spring stiffness for dynamic analysis is 10^6 to 10^{12} N/m^3, whose values are close to those in the static analysis (Liu et al. 2018).

5.3 Influences of Transverse Isotropy on Dynamic Responses

The transverse isotropy of pavement materials may affect the time and space distribution of pavement response, including surface deflection and radial strain. As one of the mechanical indexes representing the transverse isotropy of a given material, the horizontal modulus to vertical modulus ratio (k_1) of pavement materials obtained by several tests is substantially different from the isotropy assumption. Therefore, the quantitative analysis of the influence of transverse isotropy (represented by k_1) on surface deflection and radial strain is of great significance to the reasonable evaluation of pavement service life. In the subsequent analysis of transverse isotropy, the horizontal to vertical modulus ratio (k_1) for asphalt and base layer is assumed to vary from 0.25 to 1.0 (You et al. 2018; Wang et al. 2005; Ahmed et al. 2013; Rafiqul et al. 2016). The interface between asphalt and base layer is assumed changeable, whose spring stiffness (k_r) values are 10^6, 10^9, and 10^{12} N/m^3 to present the sliding, semi bonding, and full bonding conditions, respectively. In addition, when analyzing the influences of transverse isotropic of a certain layer on dynamic responses, other layers are assumed isotropic, and their properties are selected according to Table 1. Consequently, surface deflections and radial strains at the bottom of the asphalt layer are obtained, as shown in Figs. 13 and 14, respectively.

Fig. 13 shows the influences of transverse isotropy on surface deflections (t = 0.018). Surface deflection increases with a decreasing modulus ratio (k_1) of the asphalt or base layer regardless of interface contact condition. The farther from the loading center, the smaller the influence caused by the transverse isotropy of the pavement material. In addition, for the case of full bonding contact condition, the transverse isotropy of the surface layer has a greater influence on the surface deflection than that of the base layer. In the case of sliding contact condition, the transverse isotropy of base layer has the greatest effect. This phenomenon reveals the coupling influence between transverse isotropy and interface contact condition on surface deflections, which will result in a much larger surface deflection than merely considering one of them.

Fig. 14 illustrates the influence of transverse isotropy on the maximum radial strains at the bottom of the asphalt layer when t = 0.016. The transverse isotropy of the asphalt layer has a greater influence on the maximum radial strains with the same interface contact condition than that of the base layer. When the semi bonding and slip contact conditions are adopted, the maximum radial strain exhibits a decreasing trend with the increase of k_1 in the asphalt or base layer. For the full bonding contact condition, the maximum radial strain does not decrease monotonically as k_1 of the asphalt layer increases. This phenomenon reveals the coupling influence between interface condition and transverse isotropy on radial strains once again, which is similar to that in the analysis of surface deflections. Therefore, interface condition and transverse isotropy should be considered to evaluate the fatigue life of asphalt pavement properly.

6 Conclusions

Based on the wave propagation approach, a novel semi analytical solution for transversely isotropic multilayered asphalt pavement under an impact load is proposed herein. The derivation shows that the wave propagation approach can eliminate the positive exponential functions in the transfer matrix, thus avoiding overflow and ill-conditioned matrix during calculation. Moreover, the dimension of the single matrix in the presented semi analytical solution is small and has no need for the assembly of the global matrix, which contributes to a higher efficiency when more layers are included in the analysis. Generally, the proposed semi analytical solution has several advantages, such as high efficiency, no meshing, and high stability. Several conclusions could be drawn by analyzing the influence of interface bonding condition and transverse isotropy on dynamic responses:

(1) Near the loading, surface deflections and radial strains at the bottom of the asphalt layer increase with the decrease of interface stiffness. Interface stiffness has a greater influence on radial strain at the bottom of the asphalt layer than surface deflection. A higher interface stiffness results in the continuity of the radial strain between layers. When interface stiffness changes from 10^6 to 10^{12} N/m^3, it can be employed to present the sliding, semi bonding, and full bonding conditions in dynamic analysis.

(2) Surface deflection increases monotonically with the increase of the transverse isotropy of asphalt or base layer. The maximum radial strain of the asphalt layer is also greatly influenced by the transverse isotropy of the asphalt or base layer while exhibiting different trends for different interface conditions adopted. The coupling influence of transverse isotropy and interface contact condition can result in a much higher surface deflection and radial strain, which indicates that these

two parameters should be considered in the mechanical analysis and structural design of asphalt pavement.

In addition, the proposed semi analytical solution could be easily extended to the multiwheel loading and moving load analysis as well as the problems solved by the conventional TMM.

7 Data Availability Statements

Some or all data, models, or code that support the findings of this paper are available from the corresponding author upon reasonable request (part of the code and all models used in this paper).

8 Acknowledgments

This work is supported by the National Key R&D Program of China (Grant No. 2016YFE0202400) and the National Natural Science Foundation of China (Grant No. 51878228). Special appreciation is given to PhD Xin Sui and Tongxu Wang for their generous assistance in drawing the figures.

9 References

Ai, Z. Y., and Cheng, Y. C. (2014). “Extended precise integration method for consolidation of transversely isotropic poroelastic layered media.” *Comput. Math. Appl.*, 68(12), 1806-1818.

Ai, Z. Y., Feng, D. L., and Cang, N. R. (2014). “Analytical layer element solutions for deformations of transversely isotropic multilayered elastic media under nonaxisymmetric loading.” *Int. J. Numer. Anal. Methods Geomech.*, 38(15), 1585-1599.

Ai, Z. Y., Liu, C. L., and Wang, L. H. (2017). “Transient response of a transversely isotropic multilayered half-space due to a vertical loading.” *Appl. Math. Model.*, 50, 414-431.

Ahmed, M. U., Tarefder, R. A., and Islam, M. R. (2013). “Effect of cross-anisotropy of hot-mix asphalt modulus on falling weight deflections and embedded sensor stress–strain.” *Transp. Res. Rec*, 2369(1), 20-29.

Apsel, R. J., and Luco, J. E. (1983). “On the Green's functions for a layered half-space Part II.” *Bull. Seismol. Soc. Amer.*, 73(4), 931-951.

Al-Qadi, I. L., Wang, H., and Tutumluer, E. (2010). “Dynamic analysis of thin asphalt pavements by using cross-anisotropic stress-dependent properties for granular layer." *Transp. Res. Rec*, 2154(1), 156-163.

Al-Khoury, R., Kasbergen, C., Scarpas, A., and Blaauwendraad, J. (2001). "Spectral element technique for efficient parameter identification of layered media: Part II Inverse calculation." *Int. J. Solids Struct.*, 38(48-49), 8753-8772.

Al-Khoury, R., Scarpas, A., Kasbergen, C., and Blaauwendraad, J. (2001). "Spectral element technique for efficient parameter identification of layered media I. Forward calculation." *Int. J. Solids Struct.*, 38(9), 1605-1623.

Blum, K. 2012. *Density matrix theory and applications (Vol. 64)*, German: Springer Science and Business Media.

Cai, Y., and Pan, E. (2018). "Surface loading over a transversely isotropic and multilayered system with imperfect interfaces: Revisit enhanced by the dual-boundary strategy." *Int. J. Geomech.*, 18(6), 04018032.

Cai, Y., Sangghaleh, A., and Pan, E. (2015). "Effect of anisotropic base/interlayer on the mechanistic responses of layered pavements." *Comput. Geotech.*, 65, 250-257.

Caviglia, G., and Morro, A. (2000). "Wave propagation in multilayered anisotropic solids." *Int. J. Eng. Sci*., 38(8), 847-863.

Dong, Z., and Ma, X. (2018). "Analytical solutions of asphalt pavement responses under moving loads with arbitrary non-uniform tire contact pressure and irregular tire imprint." *Road Mater. Pavement Des.*, 19(8), 1887-1903.

Dunkin, J. W. (1965). "Computation of modal solutions in layered, elastic media at high frequencies." *Bull. Seismol. Soc. Amer.*, 55(2), 335-358.

Durbin, F. (1974). "Numerical inversion of Laplace transforms: an efficient improvement to Dubner and Abate's method." *Comput. J.*, 17(4), 371-376.

Erlingsson, S., and Ahmed, A. (2013). "Fast layered elastic response program for the analysis of flexible pavement structures." *Road Mater. Pavement Des.*, 14(1), 196-210.

Haskell, N. A. (1953). "The dispersion of surface waves on multilayered media." *Bull. Seismol. Soc. Amer.*, 43(1), 17-34.

Khazanovich, L., and Wang, Q. (2007). "MnLayer: high-performance layered elastic analysis program." *Transp. Res. Rec*, 2037(1), 63-75.

Kruntcheva, M. R., Collop, A. C., and Thom, N. H. (2005). "Effect of bond condition on flexible pavement performance." *J. Transp. Eng.*, 131:11(880), 880-888.

Lee, H. S. (2014). "Viscowave–a new solution for viscoelastic wave propagation of layered structures subjected to an impact load." *Int. J. Pavement Eng.*, 15(6), 542-557.

Lin, G., Han, Z., and Li, J. (2013). "An efficient approach for dynamic impedance of surface footing on layered half-space." *Soil Dyn. Earthq. Eng.*, 49, 39-51.

Liu, H., and Pan, E. (2018). "Time-harmonic loading over transversely isotropic and layered elastic half-spaces with imperfect interfaces." *Soil Dyn. Earthq. Eng.*, 107, 35-47.

Liu, H., Pan, E., and Cai, Y. (2018). "General surface loading over layered transversely isotropic pavements with imperfect interfaces." *Adv. Eng. Softw.*, 115, 268-282.

Luco, J. E., and Apsel, R. J. (1983). "On the Green's functions for a layered half-space Part I." *Bull. Seismol. Soc. Amer*., 73(4), 909-929.

Maina, J., and Matsui, K. (2005). "Elastic multi-layered analysis using DE-integration." *Publ. Res. Inst. Math. Sci*., 41(4), 853-867.

Mesgouez, A., and Lefeuve-Mesgouez, G. (2009). "Transient solution for multilayered poroviscoelastic media obtained by an exact stiffness matrix formulation." *Int. J. Numer. Anal. Methods Geomech*., 33(18), 1911-1931.

Mousa, M., Elseifi, M. A., Elbagalati, O., and Mohammad, L. N. (2019). "Evaluation of interface bonding conditions based on non-destructing testing deflection measurements." *Road Mater. Pavement Des.*, 20(3), 554-571.

Pak, R. Y., and Guzina, B. B. (2002). "Three-dimensional Green's functions for a multilayered half-space in displacement potentials." *J. Eng. Mech*., 10.1061/(ASCE)0733-9399(2002)128:4(449), 449-461.

Pan, E. (1989). "Static response of a transversely isotropic and layered half-space to general surface loads." *Earth Planet. Inter*., 54(3-4), 353-363.

Pan, E. (2019). "Green's functions for geophysics: A review. *Rep. Prog. Phys*., 82(10), 106801.

Papadopoulos, E., and Santamarina, J. C. (2016). "Analysis of inverted base pavements with thin-asphalt layers." *Int. J. Pavement Eng.*, 17(7), 590-601.

Schwab, F., and Knopoff, L. (1970). “Surface-wave dispersion computations.” *Bull. Seismol. Soc. Amer.*, 60(2), 321-344.

Senjuntichai, T., and Rajapakse, R. K. N. D. (1995). “Exact stiffness method for quasi-statics of a multi-layered poroelastic medium.” *Int. J. Solids Struct.*, 32(11), 1535-1553.

Tutumluer, E., and Thompson, M. R. (1997). “Anisotropic modeling of granular bases in flexible pavements.” *Transp. Res. Rec*, 1577(1), 18-26.

Wang, R. (1999). “A simple orthonormalization method for stable and efficient computation of Green's functions.” *Bull. Seismol. Soc. Amer.*, 89(3), 733-741.

Wang, L., Hoyos, L. R., Wang, J., Voyiadjis, G., and Abadie, C. (2005). “Anisotropic properties of asphalt concrete: characterization and implications for pavement design and analysis.” *J. Mater. Civ. Eng.*, 17(5), 535-543.

Yan, K., Xu, H., and You, L. (2016). “Analytical layer-element approach for wave propagation of transversely isotropic pavement.” Int. J. Pavement Eng., 17(3), 275-282.

You, L., Yan, K., Hu, Y., Liu, J., and Ge, D. (2018). “Spectral element method for dynamic response of transversely isotropic asphalt pavement under impact load.” *Road Mater. Pavement Des.*, 19(1), 223-238.

You, L., Yan, K., Liu, N., Shi, T., and Lv, S. (2019). “Assessing the mechanical responses for anisotropic multi-layered medium under harmonic moving load by Spectral Element Method (SEM).” *Appl. Math. Model.*, 67, 22-37.

Yue, Z. Q., and Yin, J. H. (1998). Backward transfer-matrix method for elastic analysis of layered solids with imperfect bonding. *J. Elast.*, 50(2), 109-128.

Zhang Y., Cheng, J. Y., Wang L., and Li Y. H. (2003). “An exact stiffness matrix method for axisymmetric problems of multi-layer viscoelastic half space under dynamic load.” *Chinese J. Comput Mech.*, 20(6), 749-755.

Zhang, Y., and Gao, Q. (2020). “Stability analysis of the mixed variable method and its application in wave reflection and transmission in multilayered anisotropic structures.” *Arch. Appl. Mech.*, 90(1), 127-146.

Zhang, Z., and Pan, E. (2020). “Time-harmonic response of transversely isotropic and layered poroelastic half-spaces under general buried loads.” *Appl. Math. Model.*, 80, 426-453.

Zhong, W. X., Lin, J. H., and Gao, Q. (2004). "The precise computation for wave propagation in stratified materials." *Int. J. Numer. Methods Eng.*, 60(1), 11-25.

Table 1. Parameters of pavement structure utilized for validation

Layers \ Parameters	E_v (MPa)	k_1 (E_h/E_v)	k_2 (G_v/E_v)	υ_v	υ_h	Density (kg/m^3)	Thickness (m)
Asphalt layer	2500	1	0.4	0.25	0.25	2100	0.18
Base layer	1000	0.5	0.4	0.25	0.25	2000	0.40
Subgrade	100	1	0.37	0.35	0.35	1900	Infinite

Fig. 1. Wave vector in a single layer.

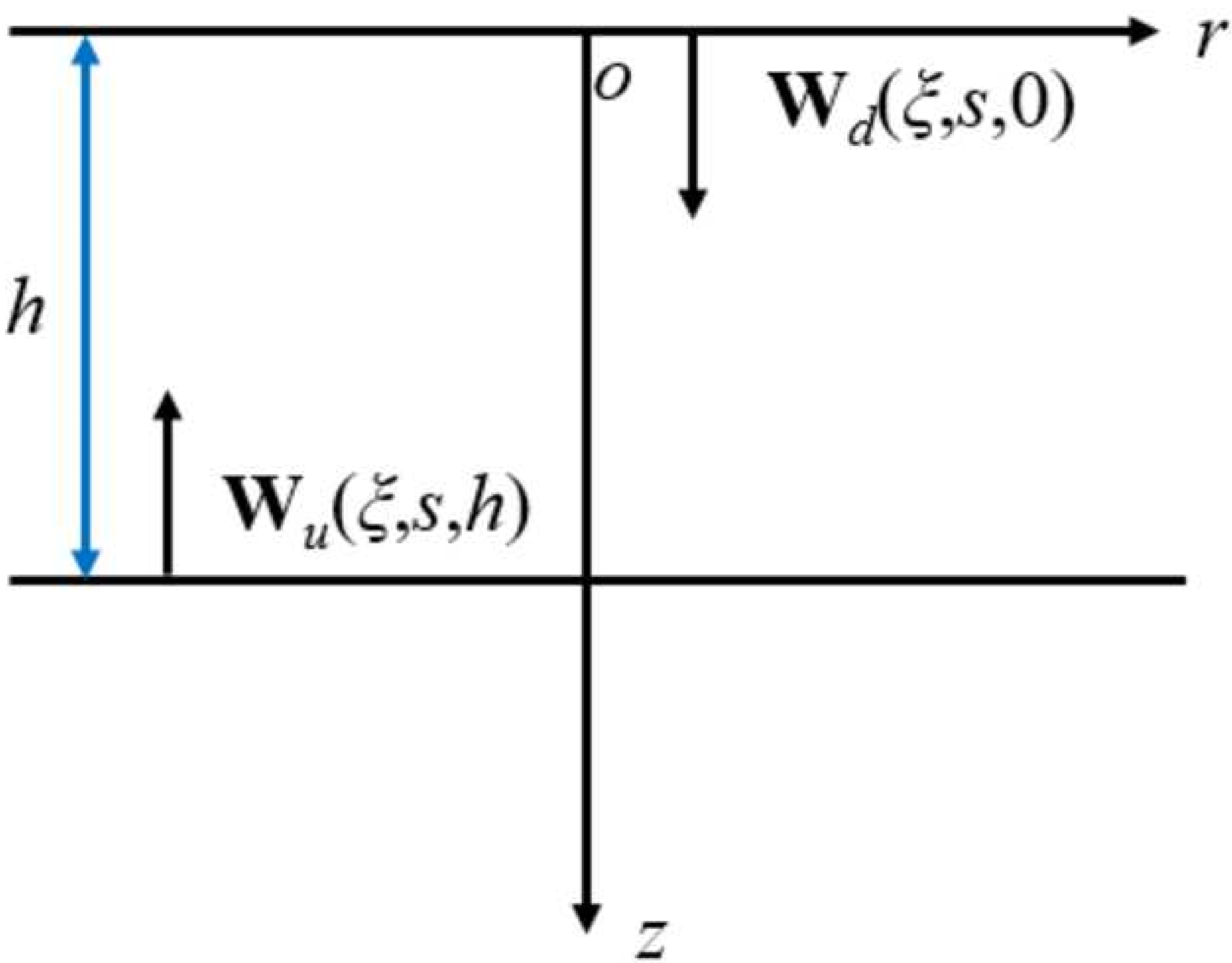

Fig. 2. A multi-layered asphalt pavement structure subjected to an impact loading

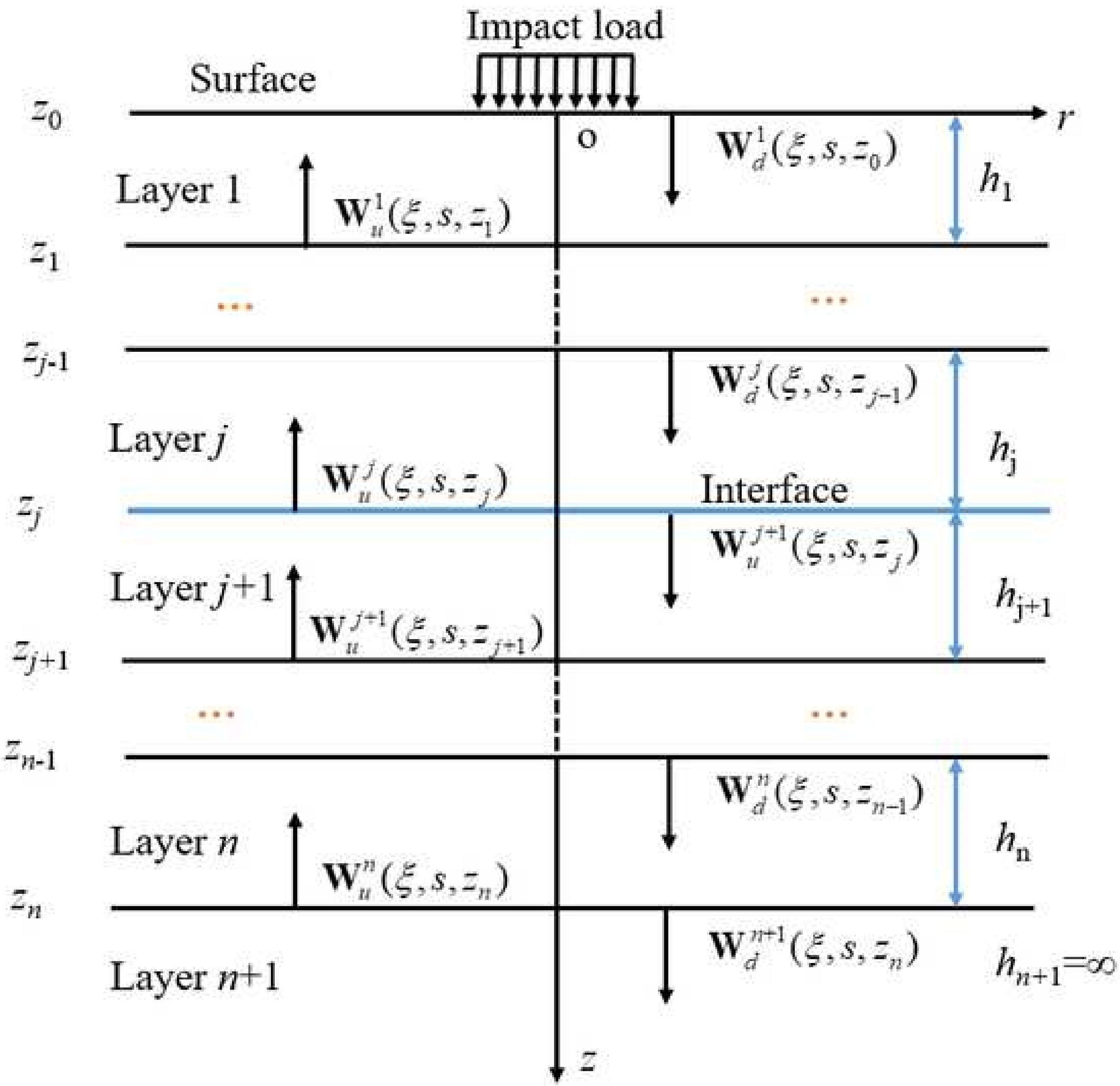

Fig. 3. Surface deflections from the reference (Al-Khoury et al. 2001) and the proposed semi analytical solution.

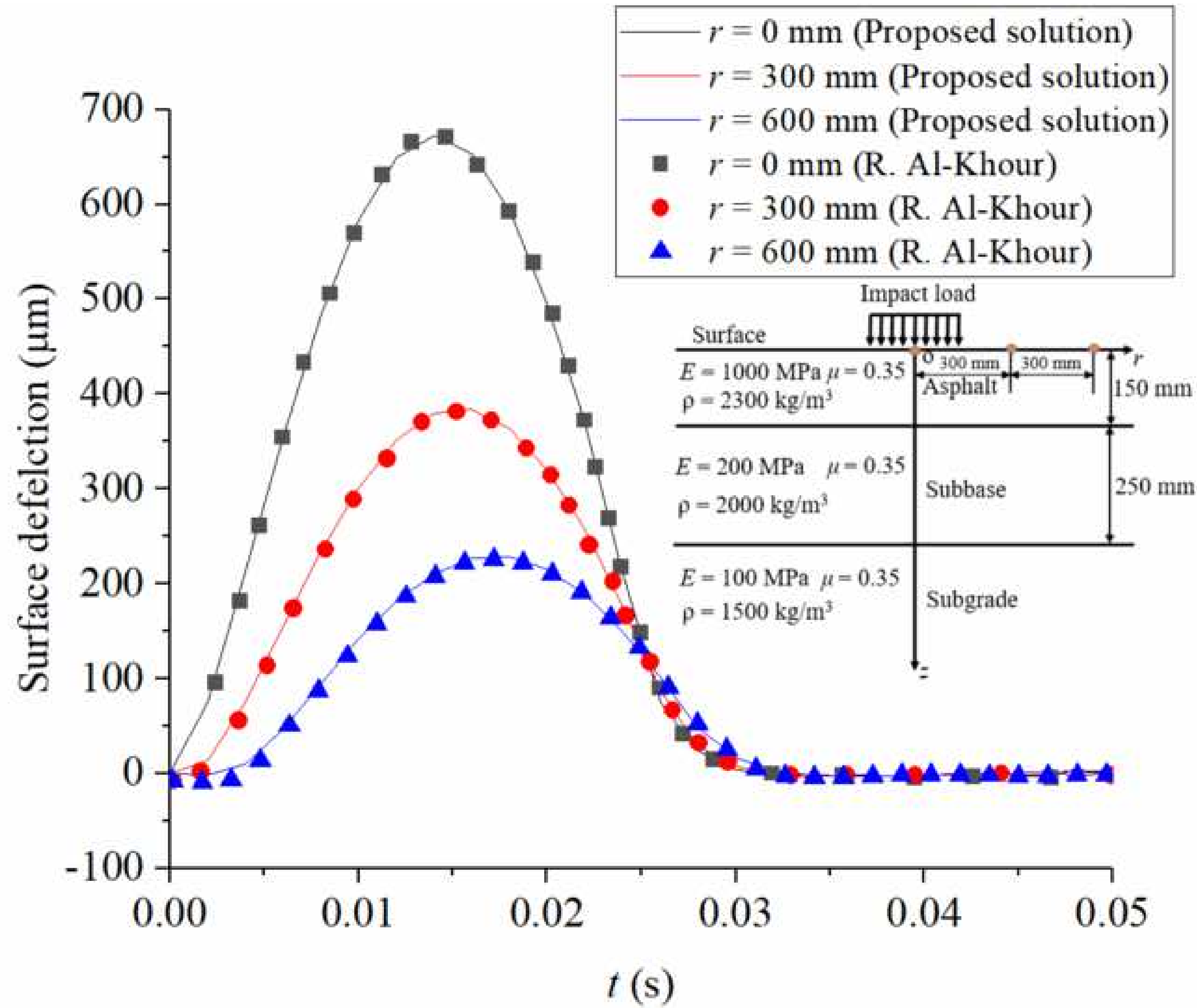

Fig. 4. Finite element model adopted in Abaqus.

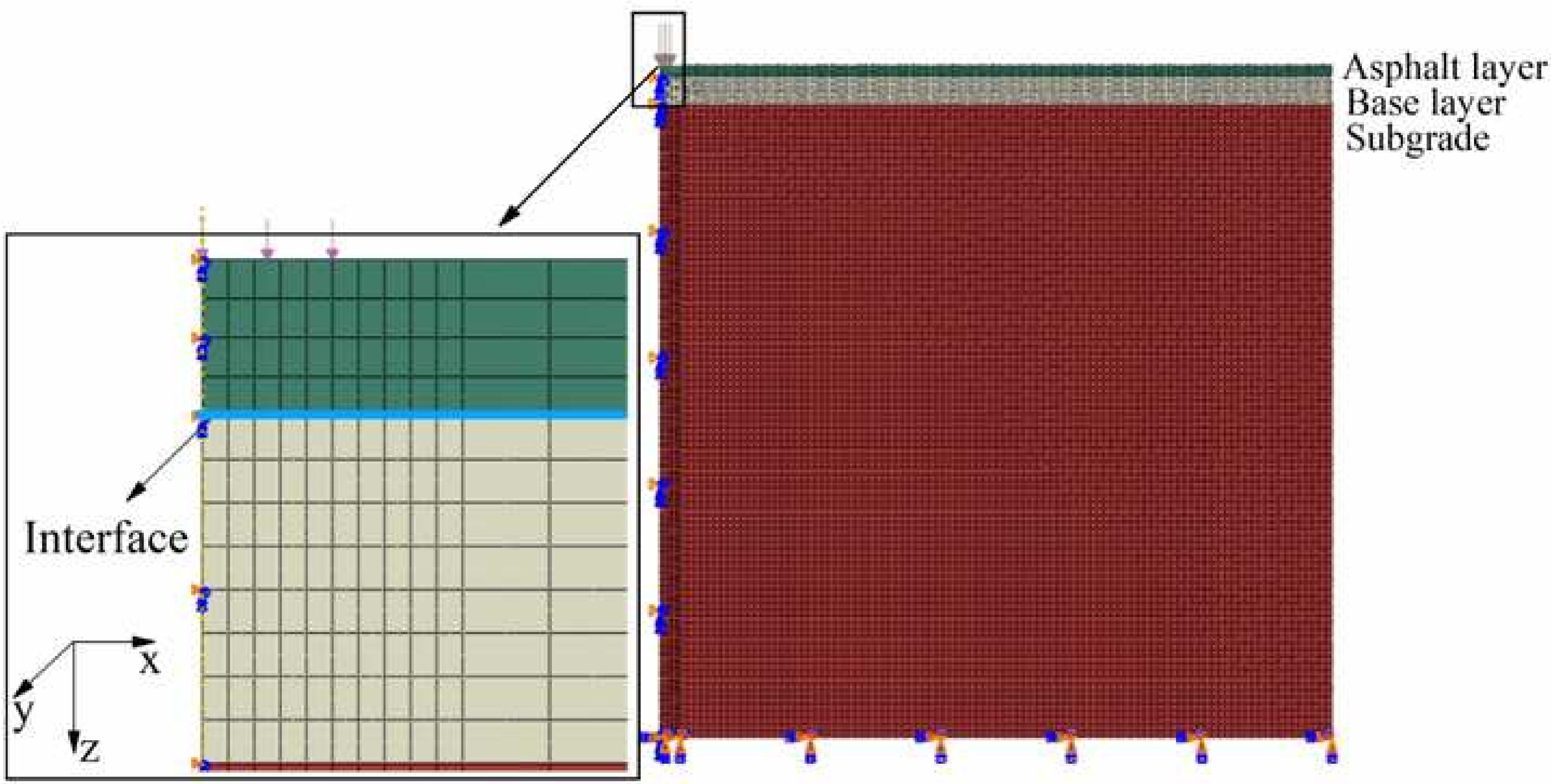

Fig. 5. Time histories of the radial strains at the bottom of surface layer under loading center.

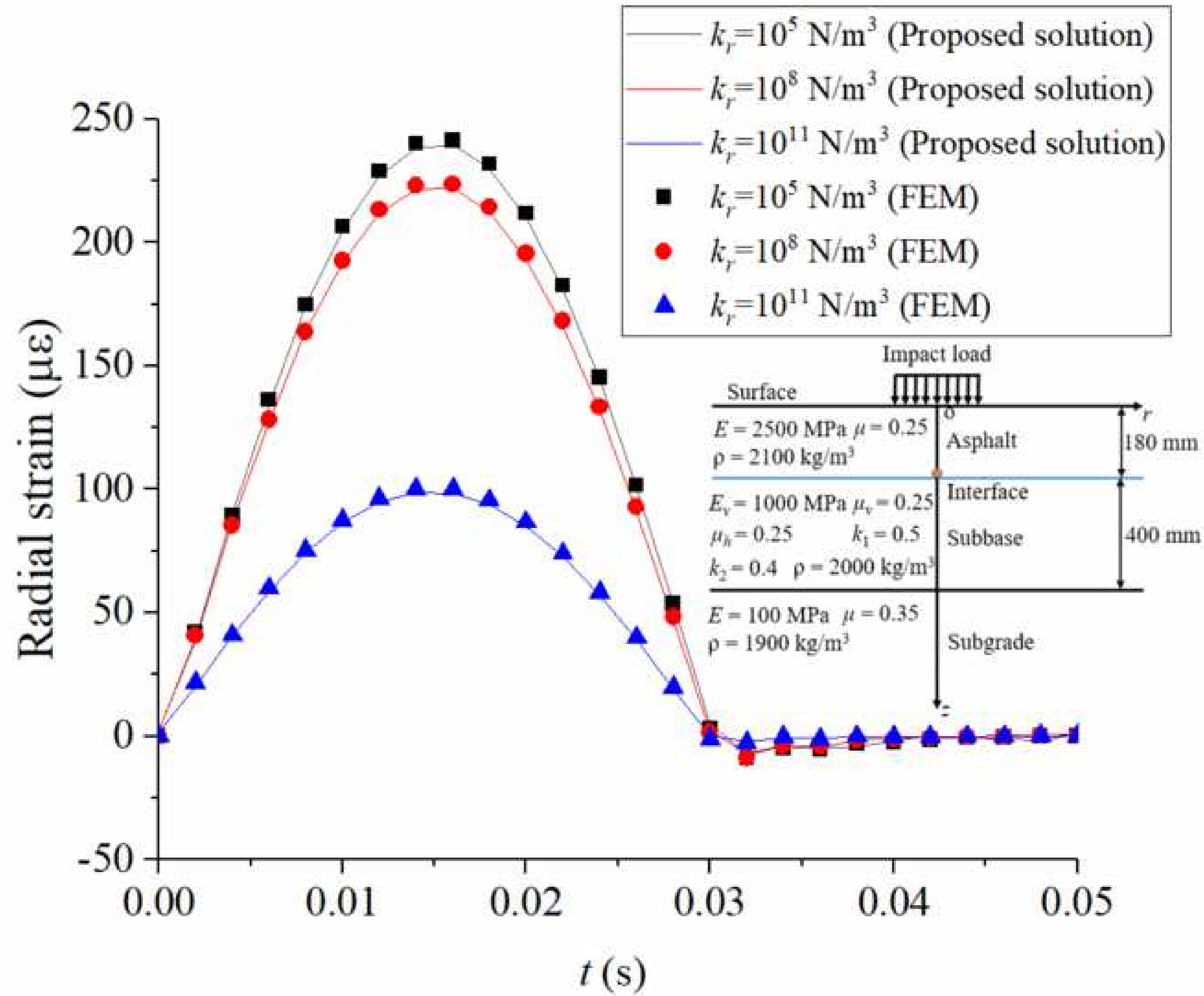

Fig. 6. Vertical strains along the z direction under loading center.

Click here to access/download;Figure;Figure 6.tif

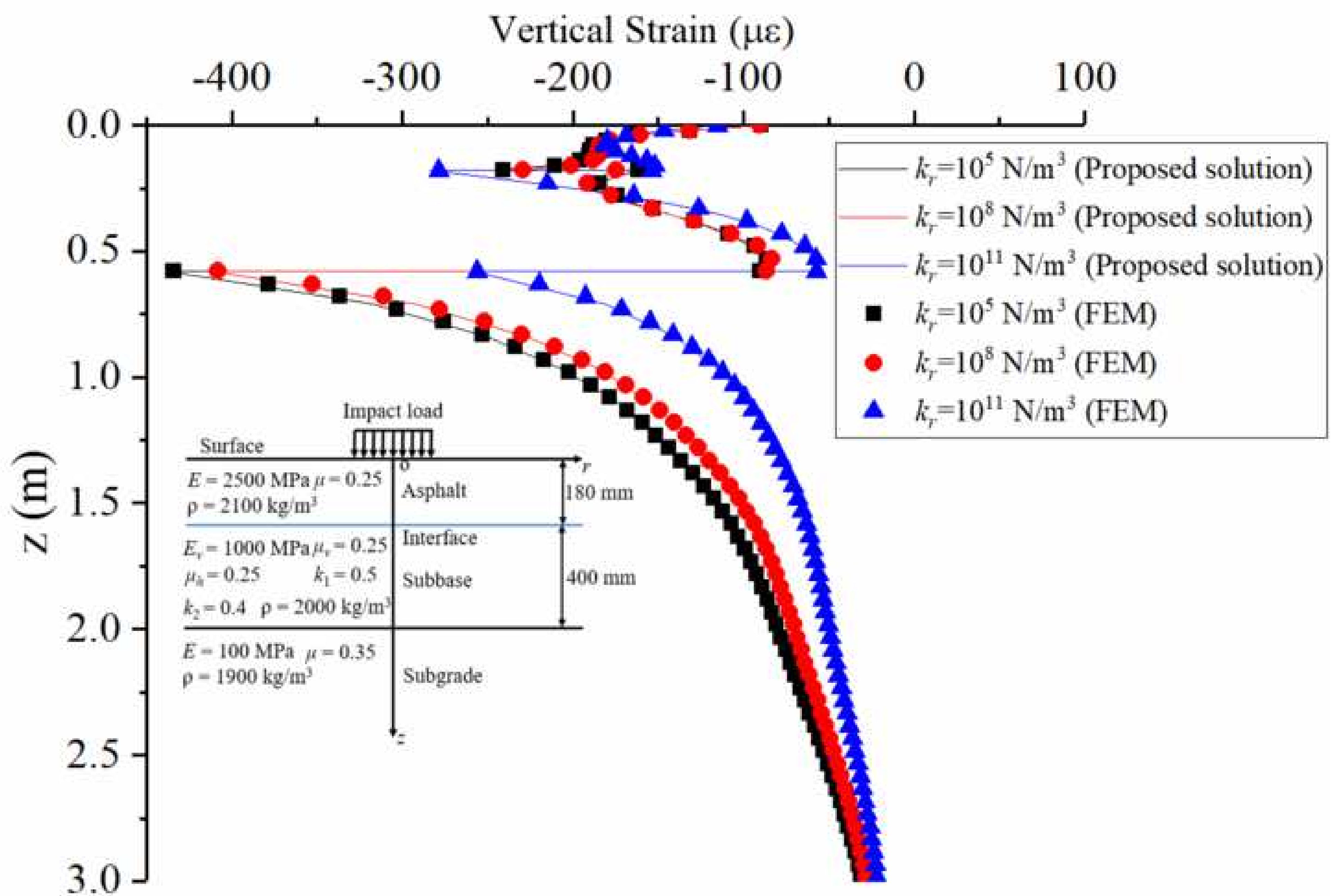

Fig. 7. Computational time for different calculating points and layers.

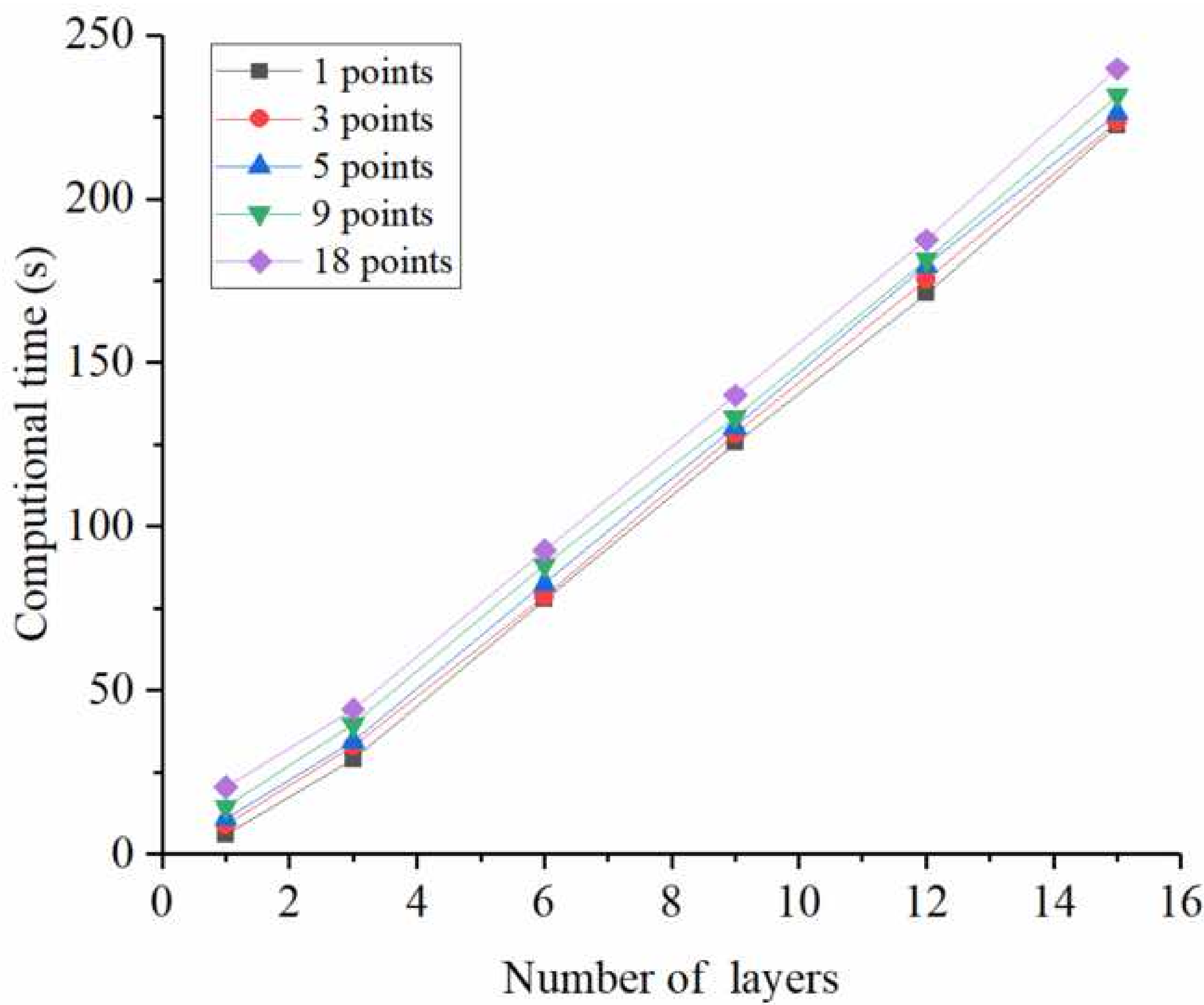

Fig. 8. Different pavement structures employed in the efficiency analysis: (a) single layer; (b) three layers; (c) six layers.

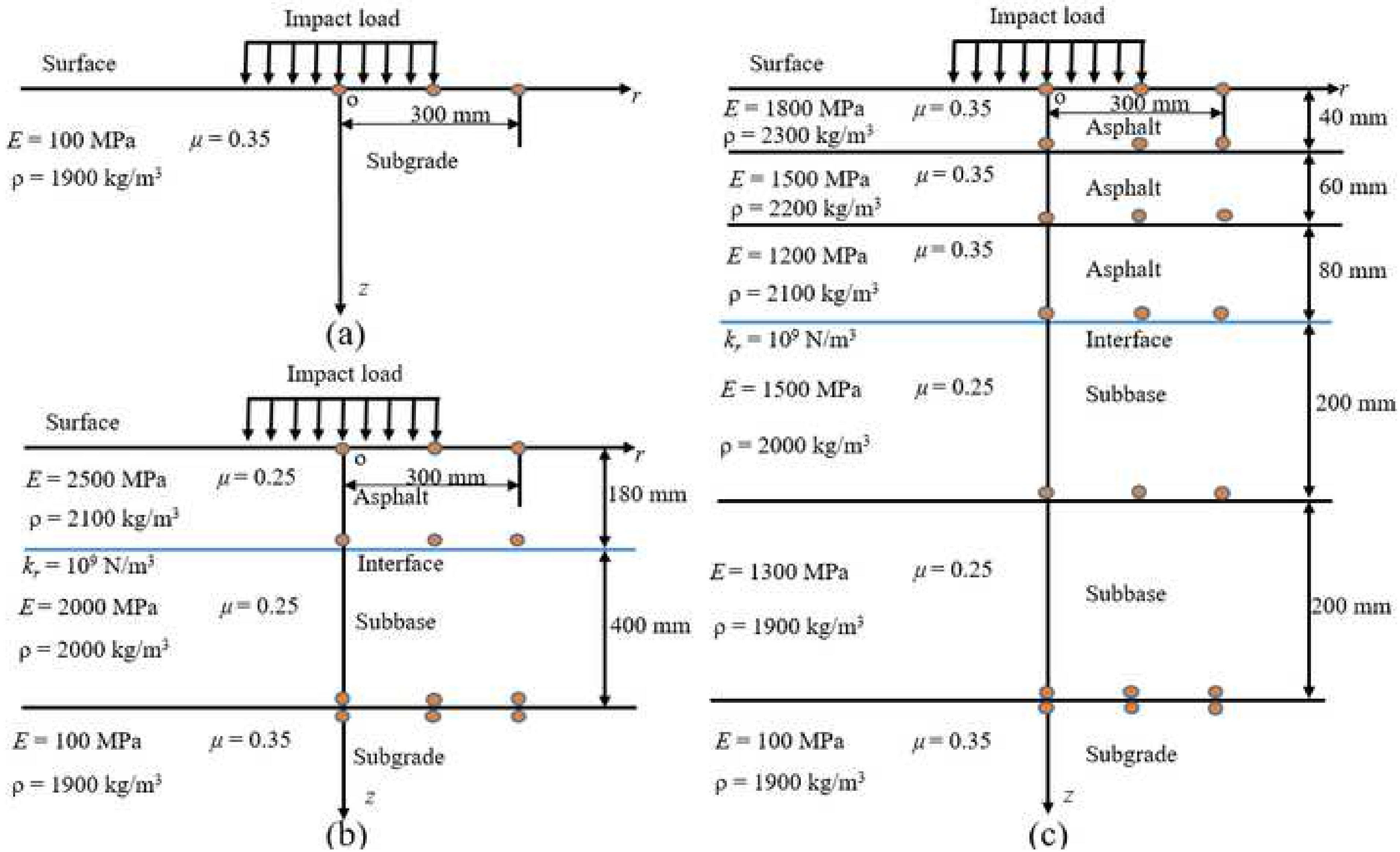

Fig. 9. Computational time of FEM and the proposed semi analytical solution.

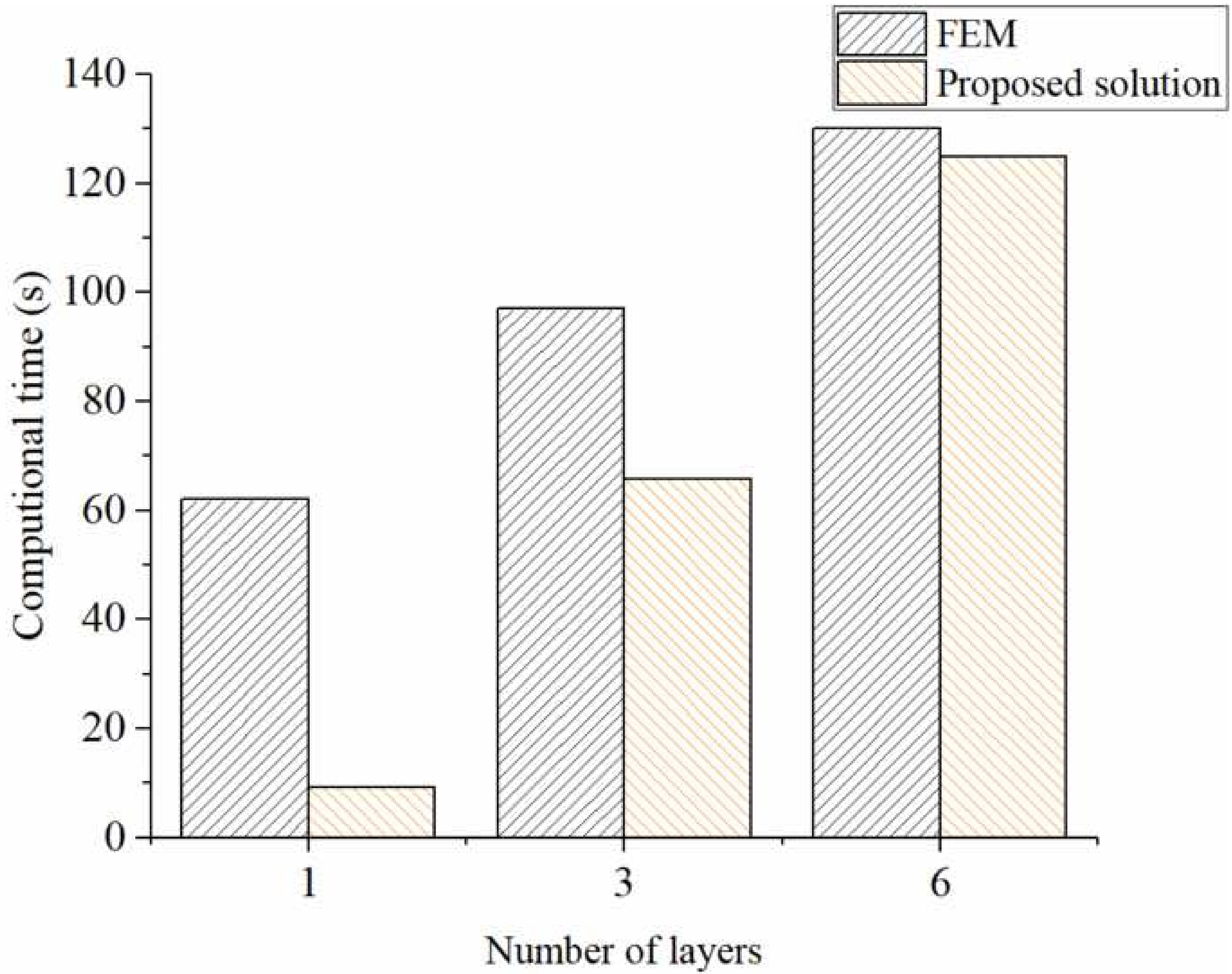

Fig. 10. Surface deflections at different radius positions with changing interface spring stiffnesses.

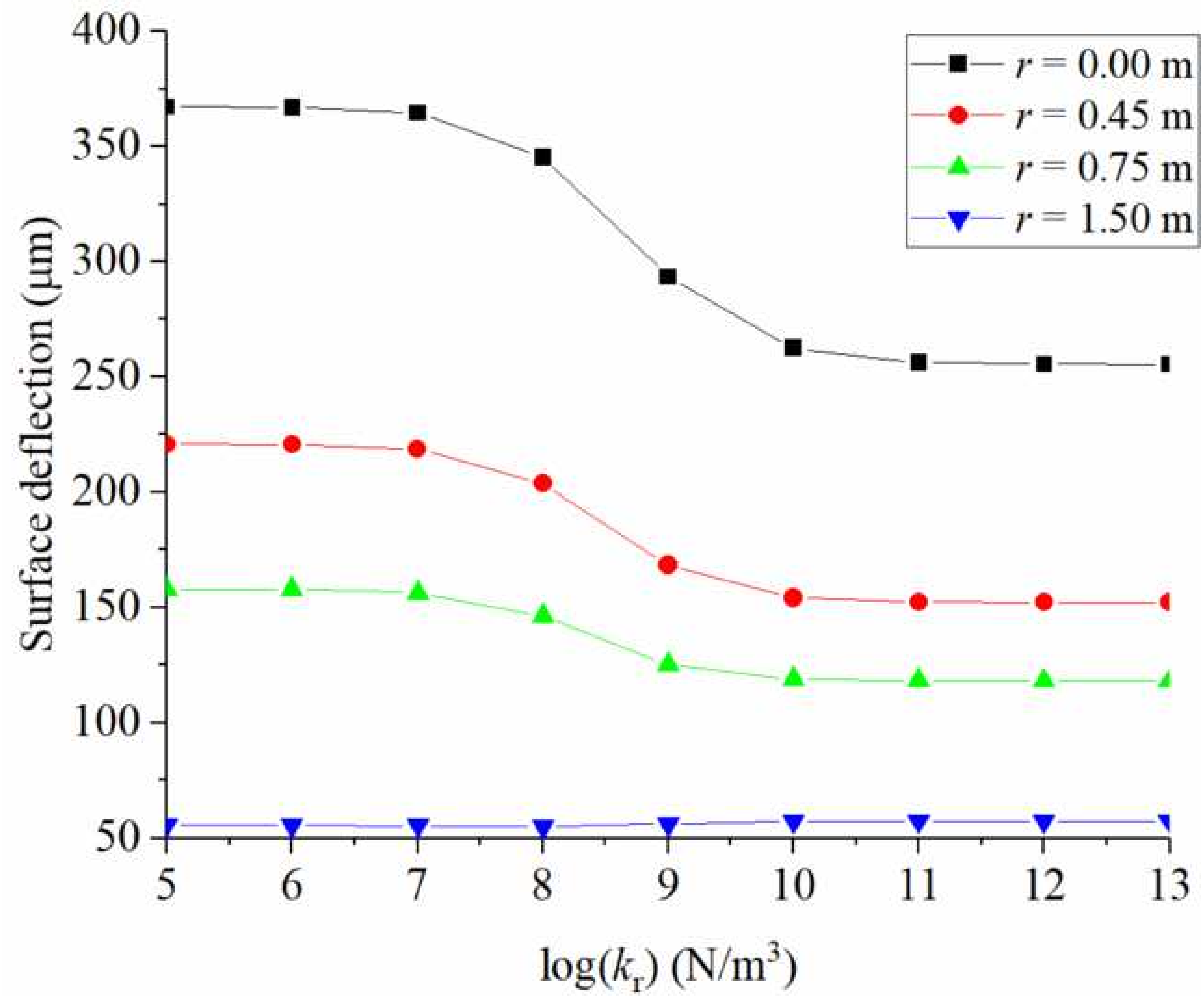

Fig. 11. Radial strains of surface layer bottom at different radius positions with changing interface spring stiffnesses.

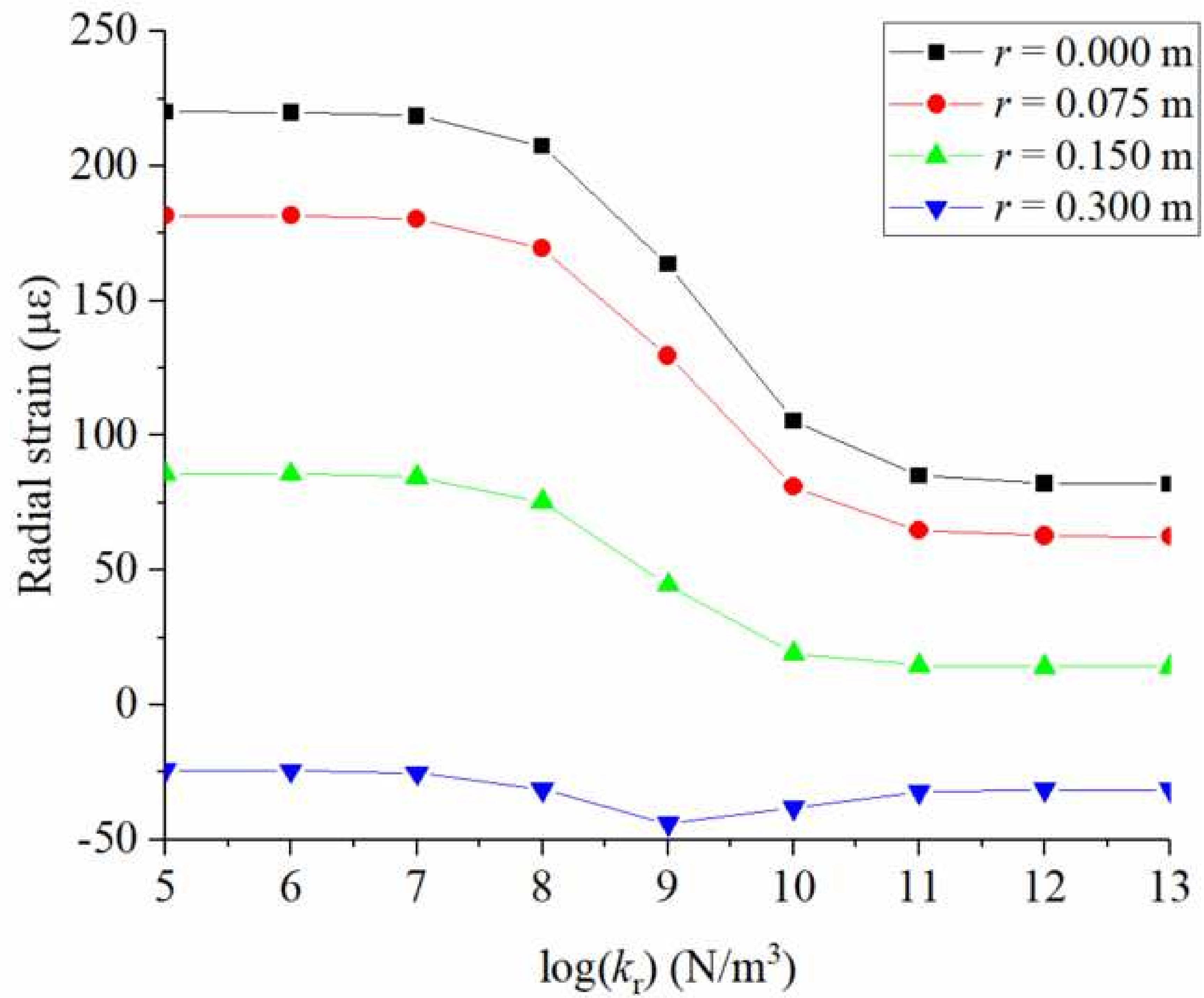

Fig. 12. Surface plots of radial strains. (a) kr = 106 N/m3; (b) kr = 1012 N/m3.

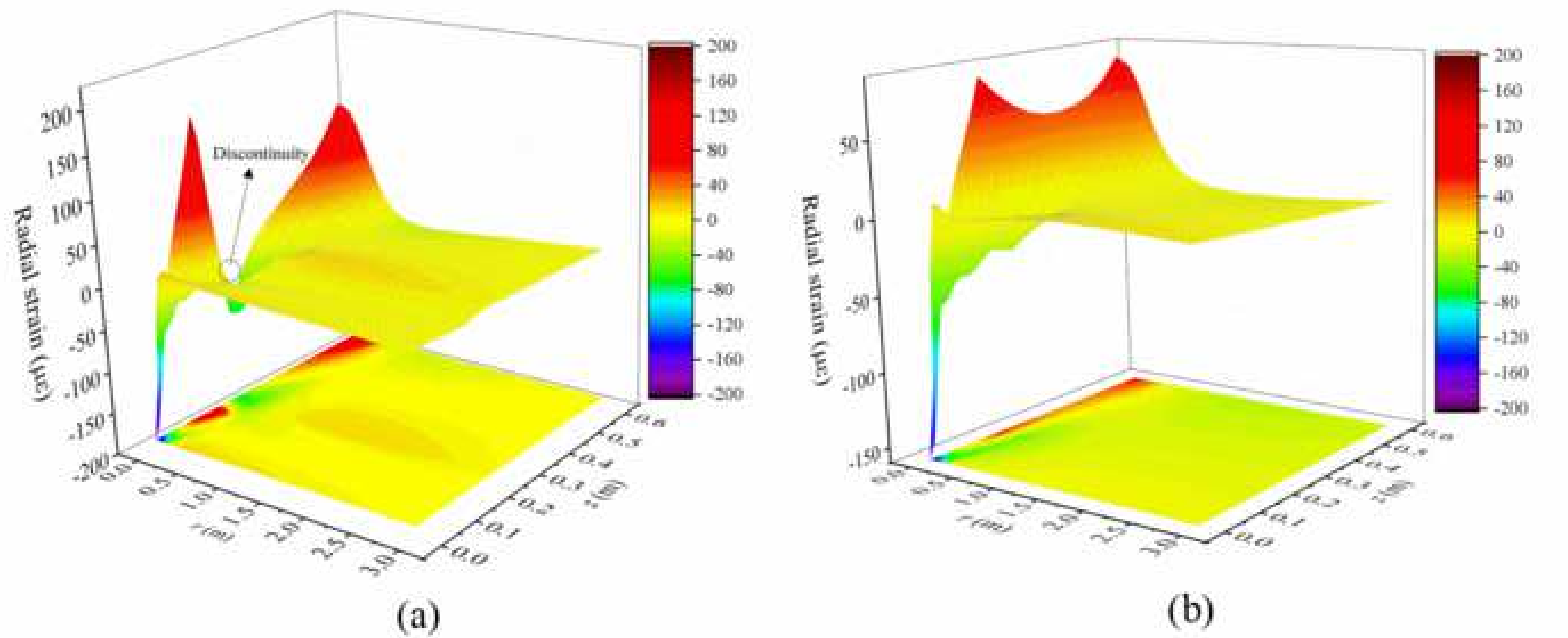

Fig. 13. Influences of transverse isotropy on surface deflections. (a) asphalt layer; (b) base layer.

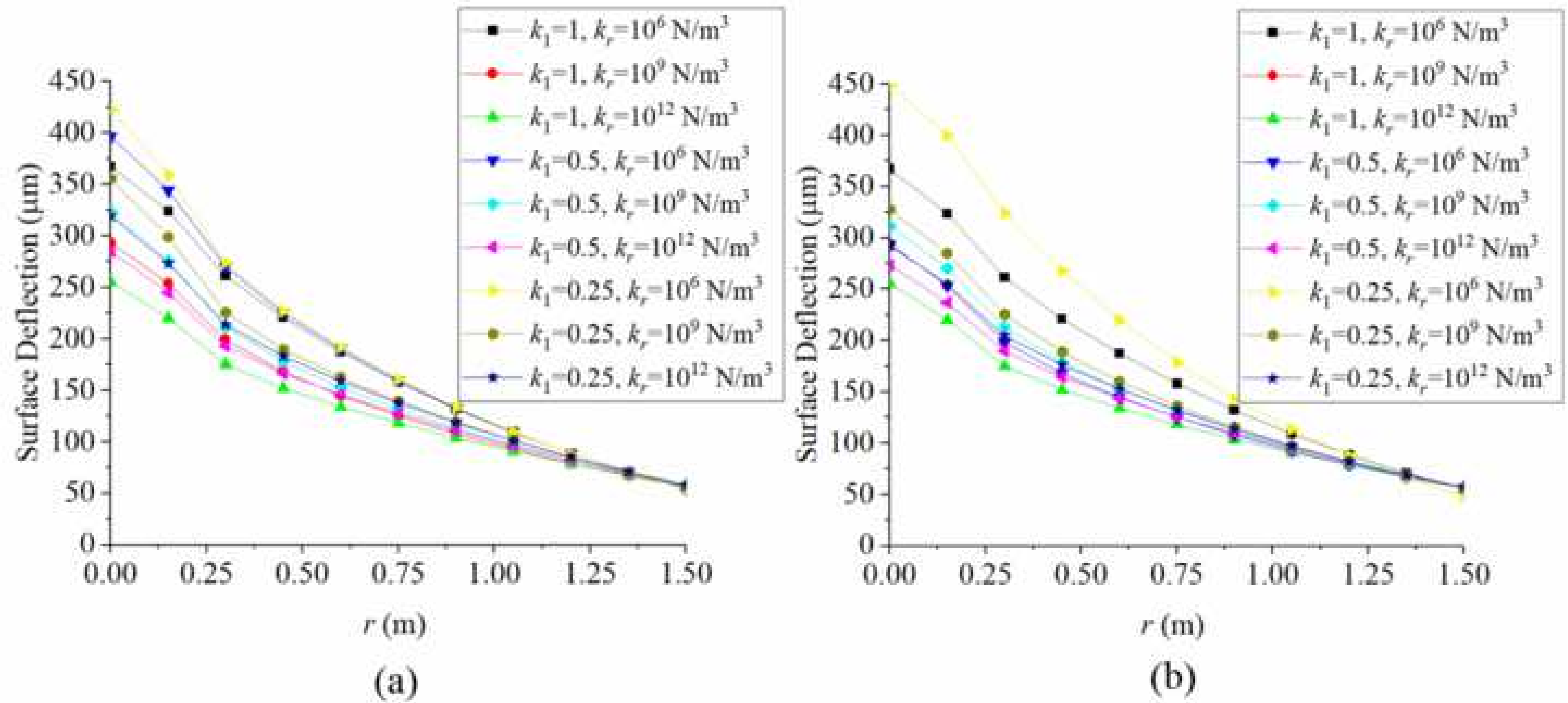

Fig. 14. Influences of transverse isotropy on radial strains of asphalt layer bottom. (a) asphalt layer; (b) base layer.

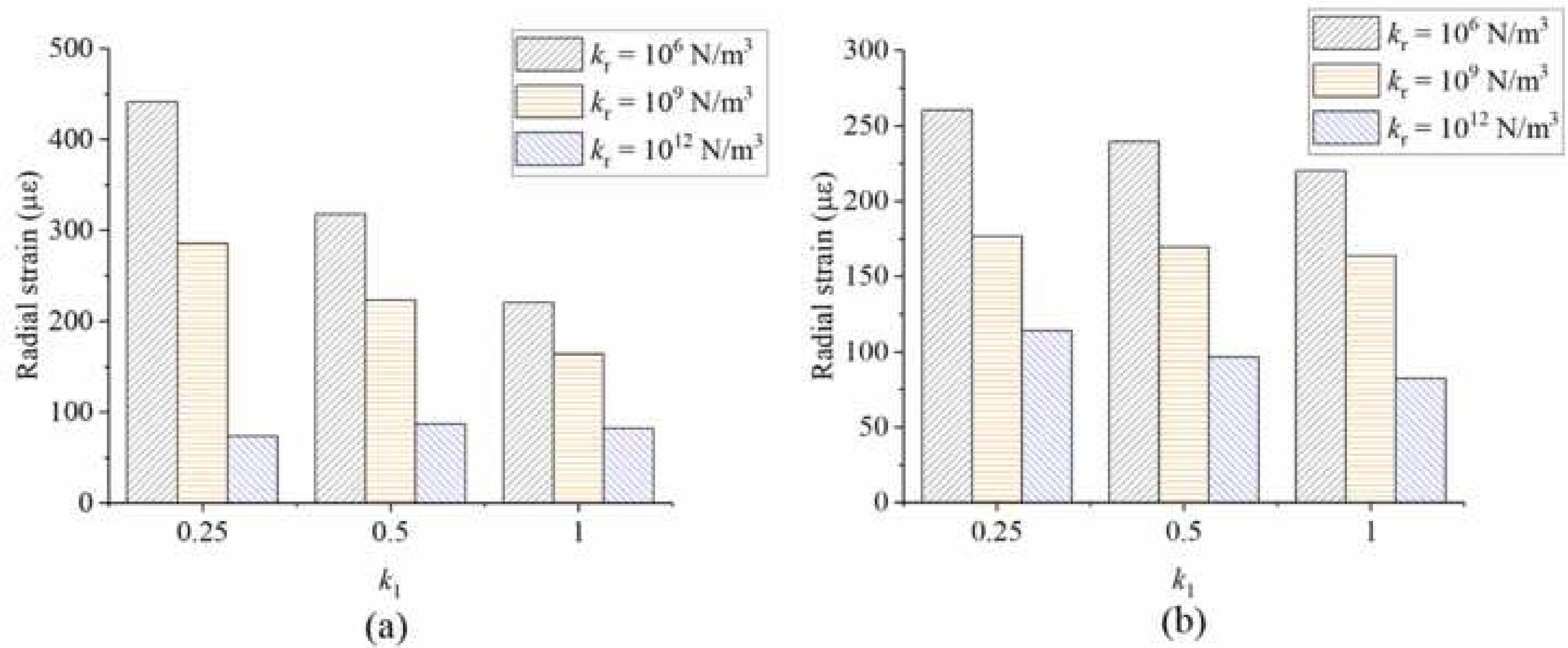

Fig. 1. Wave vector in a single layer.

Fig. 2. A multi-layered asphalt pavement structure subjected to an impact loading.

Fig. 3. Surface deflections from the reference (Al-Khoury et al. 2001) and the proposed semi analytical solution.

Fig. 4. Finite element model adopted in Abaqus.

Fig. 5. Time histories of the radial strains at the bottom of surface layer under loading center.

Fig. 6. Vertical strains along the *z* direction under loading center.

Fig. 7. Computational time for different calculating points and layers.

Fig. 8. Different pavement structures employed in the efficiency analysis: (a) single layer; (b) three layers; (c) six layers.

Fig. 9. Computational time of FEM and the proposed semi analytical solution.

Fig. 10. Surface deflections at different radius positions with changing interface spring stiffnesses.

Fig. 11. Radial strains of surface layer bottom at different radius positions with changing interface spring stiffnesses.

Fig. 12. Surface plots of radial strains. (a) $k_r = 10^6$ N/m^3; (b) $k_r = 10^{12}$ N/m^3.

Fig. 13. Influences of transverse isotropy on surface deflections. (a) asphalt layer; (b) base layer.

Fig. 14. Influences of transverse isotropy on radial strains of asphalt layer bottom. (a) asphalt layer; (b) base layer.